# 15

# *Alternative methodologies for the production of nanomaterials based on microfluidics and laser pyrolysis technologies*

**Gema Martínez[1,2], Víctor Sebastián[1,2,3] and José L. Hueso[1,2,3,*]**

[1]Institute of Nanoscience of Aragon, R+D Building, C/ Mariano Esquillor, s/n; 50018, University of Zaragoza, Spain
[2]Networking Research Center on Bioengineering, Biomaterials and Nanomedicine, CIBER-BBN, 28029 Madrid, Spain
[3]Department of Chemical Engineering and Environmental Technology, University of Zaragoza, Spain

## Outline:

# Introduction

The superior properties of nanomaterials will promise a revolutionary new approach with a major impact in a wide variety of innovative applications, ranging from catalysis to photonics and optoelectronic, from energy production to thermal management. These improvements stem from structural features such as particle size or layer thickness on a scale 1-100 nm, much smaller than that found in bulk materials. Additionally, biological systems are considered as the ideal playground for nanoparticle (hereafter denoted as NP) applications. Therefore, the screening and synthesis of new nanostructured materials is a major research topic in the development of the nanotechnology field. NPs of a wide range of chemical compositions and phases can be prepared by a variety of methods; however the production of large amounts of pure, non-agglomerated NPs, with desired size and narrow size distribution, is still an extremely difficult task [1].

This chapter overviews different approaches for the synthesis of nanostructured materials based on alternative methodologies to the most conventional and widespread colloidal wet chemical routes and with a great potential applicability to large-scale and continuous production of nanomaterials. Microfluidics and laser-assisted pyrolysis technologies are fully described. Their major outcomes, present state-of-the-art and potential applications for the next future are reviewed. The major advantages of microreactors include favorable surface area-to-volume ratios and increased driving forces for heat and mass transport. A more exquisite control and miscibility of reactants, reduces costs, time and enhances reproducibility from batch-to-batch strategies. Laser pyrolysis also exhibits several advantages, such as high quality and purity of the products obtained due to the reduction of side reactions, a continuous process capable of high yields that avoids the intrinsic variability of batch processing, and ability to tune nanoparticle properties by adjusting the process parameters.

### *Microfluidic Technology*

### *Microfluidics Fundamentals*

Continuous flow reactors based on microfluidics constitute an upcoming technology of highest potential for liquid phase synthesis of nanomaterials. This technology overcomes the inherent drawbacks which batch synthesis reactor suffers from: lack of reproducibility of size, wide size distribution, lack of quality of the nanomaterials from batch to batch and scale-up difficulties.[2, 3] Sufficient mixing and rapid mass transfer can significantly improve these parameters, which in turn control both the physical and chemical properties of nanoparticles. Microfluidic technology takes advantage of the large surface area-to-volume ratios within microchannel structures to accelerate heat and mass transport. Microfluidic systems offer large interfacial areas per unit volume (10,000–50,000 $m^2/m^3$) which is much higher than the surface area-to-volume ratio of conventional reactors (100 $m^2/m^3$)[4]. This accelerated transport allows for fast changes in reaction temperatures and reagent concentrations, originating a more uniform heating and mixing which can have dramatic impacts on macromolecular yields and nanoparticle size distributions[4]. Furthermore, microfluidic technology brings up some interesting advantages to the nanomaterials field, including enhancement of mass and heat transfer, feedback control of temperature and feed streams, reproducibility, rapid screening of synthesis parameters, and low reagent consumption during the optimization process because of the small volume reactor.[2] These advantages enable nanoparticle synthesis reactions to be performed under more aggressive conditions with higher yields than can typically be achieved with conventional batch reactors.[2] Novel nanomaterials can be produced since it is feasible to work at elevated temperatures and pressures while confining potentially toxic, high reactive starting materials.[2]

Microfluidic reactors offer modular design, with the possibility of increasing the number of modules to adapt to the specific process requirements[3]. Microfluidic technology brings the possibility of synthesizing nanomaterials at the point-of-use[4]. This eliminates the need to store and transport hazardous materials and provides an ease handling of nanoparticles prone to ageing or phase transformation, dependent on the local conditions, or are not economically amenable for large-scale production. Scaling the production by "numbering up" (arraying parallel microreactors) enable capital investment and market growth to be coupled, reducing financial risk, which is valuable in emerging areas such as nanotechnology.[5]
Microfluidic reactors are continuous-flow chemical synthesis reactors typically containing a network of miniaturized flow channels under the millimeter range. The network of channels designed to maximize the reaction performance towards the desire nanomaterial shape, composition or size distribution. Microfluidic reactors have evolved from simple tubing[6] to complex and sophisticated systems integrating control of operating parameters and in situ characterization techniques in a chip.[7]

***Fabrication of Microreactors***

*Type of reactors.* Continuous flow microreactors can be categorized into two groups: the simplest capillary tubes constructed by mechanical assembly and more sophisticated on-chip microchannel networks[4]. The main challenge in using microfluidic reactors to nanoparticle synthesis is to design microsystems capable of producing the desired solid materials at the desired conditions without the reactor clogging.[2] The chemical and physical properties of the nanomaterial selected as target will influence in the microfluidic reactor design: material used for reactor construction, microchannels arrangement, reagents addition, pressure, temperature and solvent affinity.

*Tubing systems* that operate by using capillary tubings for the flow of fluids could be considered as tubular flow systems but with dimensions of microns. Capillary tubings are usually made of stainless steel, silica or polymers depending on the wettability required, as well as the mechanical requirements established to endure at the synthesis conditions. They are used in preliminary test to access small scale flows within the simplest feature. Furthermore, they provide cheap and simple approaches for continuous flow experiments with well-known hydrodynamics based on dispersed plug-flow models[8]. This type of reactor enables an easy manipulation of operating parameters such as residence time or temperature [9], but under some synthesis conditions it could arise mixing limitations that could not enable the proper size distribution[10]. Though the capillary tube reactors have several advantages such as flexibility and simplicity in operation, they are frequently prone to problems such as clogging or blockage of reactor channels and may lead to broader particle size distributions.[11] These drawbacks were faced in some cases by using coaxial tube reactors or segmented flows, where two immiscible liquids with laminar flow resulting in the formation of droplets of the reactant solution that avoids the contact of the reacting phase with the reactor walls[10] (see figure 15.1 a-b). Synthesis of inorganic nanomaterials using capillary tubes made from stainless steel[12], silica glass[9], and polymers like PTFE[6] have been reported.

*Chip-based flow systems*. Chip-based flow systems are devices that integrate multiple functions. As a result of advances in microfabrication processes, several materials can be chosen among for building chip-based flow systems. Depending on the constrains imposed by the type of applications and operating conditions, they can be fabricated from various materials such as glass, silicon, stainless steel, metals, and polymers[13]. Glass has been the most popular material since it is chemically inert to most reagents and solvents. The transparency of glass enables the visual inspection of microchannels in

order to detect a fouling process and fabrication procedures are well established[14]. The low thermal conductivity of glass limits applications requiring good heat transfer.

Silicon has also found widespread use in the fabrication of microreactors, since methods developed for semiconductor chip production can be applied to create a variety of three-dimensional layouts[15]. Silicon and oxidized silicon, like glass, are chemically inert to most reagents and solvents, which grant silicon based reactors with outstanding heat-transfer capabilities. Exothermal reactions that require a fast heat removal as well as reactions that require very high or low temperatures benefit from silicon microreactors[16]. Silicon technology is undoubtedly the most advanced manufacturing technology. Structuring by lithography and subsequent etching (wet and dry etching) allow structures to be carved into wafers with high precision at the micron range (see figure 15.1-c).

Stainless steel is the standard material for process chemistry and, stainless steel chip-based reactors have been developed, including modular systems such as micromixers and heat exchangers [17] (see figure 15.1-d). Stainless steel microreactors are typically fabricated using conventional machining, electroforming, electro-discharge machining (EDM), or laser ablation[2]. The dimensions of these reactor systems are generally larger than those of glass and silicon reactors because the resolution of the fabrication techniques is less accurate than the ones applied in glass or silicon. Stainless steel based flow chips are especially advantageous for processes involving high heat load and toxic reagents thanks to good chemical compatibility and thermal resistance of stainless steel, except for synthesis process where strong acids are involved[2].

Polymer-based microflow systems made of polymers such as poly (dimethylsiloxane) (PDMS) are relatively inexpensive and easy to produce. The huge variety of plastics materials, displaying a wide range of properties, covers a gap in micro-system manufacturing. The chips replication is very cheap, but many solvents used for non-aqueous nanoparticle synthesis are not compatible with these polymers that show limited mechanical stability and low thermal conductivity. Consequently, the application of these reactors is mostly restricted to aqueous wet-chemistry methods at atmospheric pressure and mild temperatures[21]. Their fabrication is made following the popular soft lithography technique[22], where a negative photoresist is used to prepare a master chip, followed by the silicon elastomer casting onto this mold and further curing. The PDMS layer is peeled off and bonded to a glass slide to seal the channels[2]. There are some prominent replication technologies such as hot embossing and microinjection molding. Some new polymers have been applied in polymer-based chips in order to overcome the drawbacks of PDMS. For instance, SU-8-PEEK microreactors have been developed for nanomaterials synthesis based processes up to 150 ºC and pressure up to 2 MPa[23].

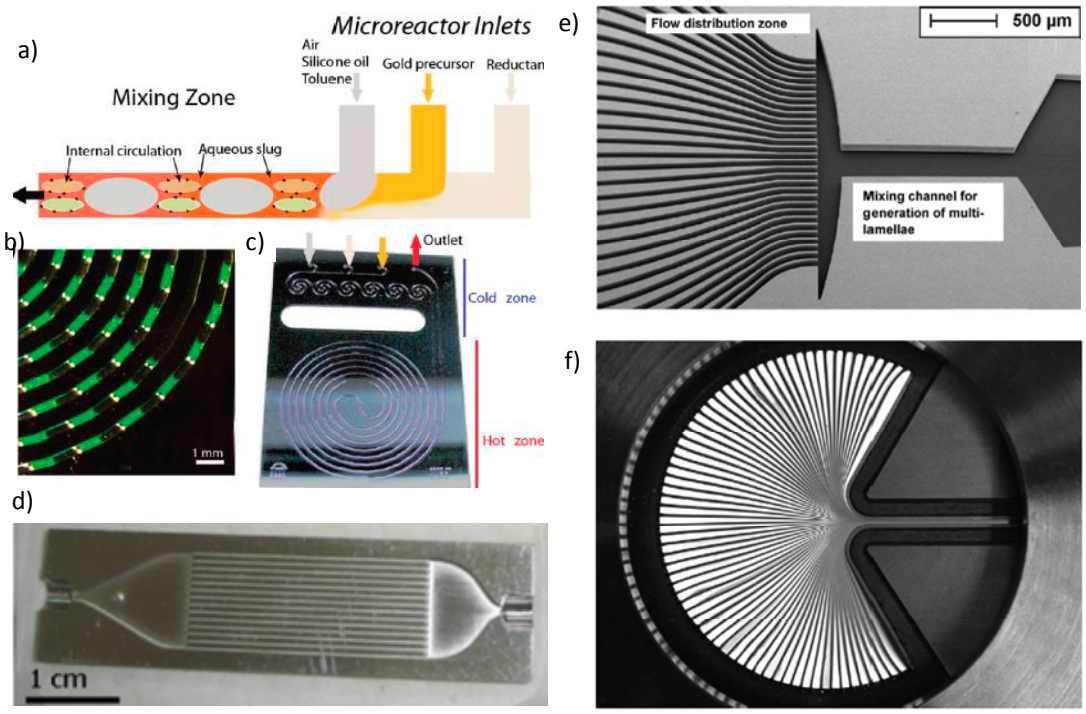


**FIGURE 15.1**
(a) Schematic of the segmented flow generation in a microreactor. (b) Detail of segmented slugs generated at a hydrophilic microfluidic reactor. The aqueous slug (continuous phase) contains fluorescein (green color); the disperse phase is toluene. (c) Spiral silicon/Pyrex microfluidic reactor designed at MIT for gold nanocrystal synthesis. Reprinted with permission from ref. 10; d) Stainless-steel microreactor designed by IMM. Reprinted with permission from ref. [18]; d) Slit-type interdigital micromixer made in glass for laboratory-scale applications, typical liquid flows 10–1000 ml/h. Reprinted with permission from ref. [19]; e) Multi-lamination pattern fed by 138 microchannels in a SuperFocus mixer made of stainless steel and equipped with an inspection window. Reprinted with permission from ref. [20]

Chip-based flow systems usually contain microchannels, which allow small volumes of reagents to flow, mix and react under an exquisite environment control. They also integrate various components such as micropumps[24], micromixers[17], microvalves[25], microheaters[26], optical or electrochemical sensors[27]. The continuous operation mode allows sophisticated control of reactions, for instance, secondary reactions can be started or quenched at a certain reaction time by adding reagents from certain spatial positions downstream. For nanoparticle engineering,allows the growth multi-layer nanostructures. Macroscopic devices usually enhance the diffusional mixing activity by turbulent stirring or shaking, which is not feasible in microflow systems, where the operation conditions are usually under laminar flow. Micromixers instead use appropriate channel geometry to establish large contact-surface-to-volume ratios between streams, for example, by following a multilamination strategy (see figure 15.1 e-f). The diffusion time strongly depends on the diffusion length (diffusion time = [diffusion length]$^2$/[diffusion coefficient]). Then, the smaller the microchannel diameter, the faster is the mixing. The strength of micromixing is particularly important in multiphase applications. For instance, the capability to produce very uniform emulsions on an industrial scale has been demonstrated by using micromixers[28]. Heat transfer is governed by the same principles that mass. The speed of thermalization within the reactors

improves with shrinking micro-channel diameters, and most importantly the heat flow through increases as the wall thickness diminishes. An integrated microchannel heat exchanger, for instance, could provide heat transfer coefficients up to 26,000 $W/m^2$ K, which is an order of magnitude higher than conventional heat exchangers[4]. This fact makes that a fast and accurate temperature control could be achieved for nanoparticle synthesis. In general, it takes only seconds or sub-seconds to raise a solution in a microchannel from room temperature to hundreds of degree[4]. Consequently, the successful fabrication of microflow systems must handle both properties of materials and design parameters in order to fulfill the expected requirements.

***Laser Pyrolysis***

Developing methods for the synthesis of nanoparticles are taking place in colloid systems where stabilization of the as-prepared nanoparticles is used to prevent coagulation. However, gas-phase processing systems are better in some cases because of their following inherent advantages:

(i) Gas-phase processes are generally cleaner than liquid-based processes since even the most ultra-pure solvent contains traces of minerals or impurities, detrimental such as electronic grade semiconductors. These impurities seem to be avoidable today only in vacuum and gas-phase systems.
(ii) Gas-phase processes have the potential to create complex chemical structures which are useful in producing multicomponent materials of a broad range of complex compositions, such as high-temperature semiconductors.
(iii) Particle size crystallinity , degree of agglomeration, porosity, chemical homogeneity, stoichiometry all this properties can be relatively tuned up by either adjusting the process parameters or adding an extra processing step, e.g. sintering or size fractioning.
(iv) Gas-processes for particle synthesis are usually continuous process, while liquid-based synthesis processes or milling process are often performed in a batch form. Batch processes can result in product characteristics which vary from one batch to another.

The laser pyrolysis technique is usually classified as a vapor-phase synthesis process for the production of nanoparticles. At the beginning of the 80`s, Cannon et al [29] first reported laser pyrolysis as a method for producing highly uniform silicon nano-powder. Later, in the middle of the 80's, the laser pyrolysis technique was used to study the gas-phase thermal decomposition of iron pentacarbonyl $Fe(CO)_5$ and metal hexacarbonyl complexes $M(CO)_6$ of Cr, Mo and W [30 31]. This highlights the versatility of the technique as a synthesizing method. The advantages in this technique include: a well defined interaction volume, spatial uniformity of the reaction zone, short millisecond scale residence times, high heating/cooling rates, no interaction with the reactor chamber walls to minimize the presence of impurities and the attainment of very fine particles [32].
This overview shows laser pyrolysis technique to be one of the most powerful and versatile gas-phase technique for producing nanostructures of various chemical compositions in the range 2-200 nm in average particles size with remarkably narrow distributions, which can be used for promising structural and functional applications.

*Model Processing.* The principle of the method is based on the decomposition of reactants by a high-power infrared (IR) $CO_2$ laser followed by a quenching effect. In this category of synthesis routes, nanoparticle formation starts suddenly when a sufficient degree of supersaturation of condensable products is reached in the vapor phase. This includes a vapor phase that is thermodynamically unstable

relative to formation of the solid material to be prepared in nanoparticles form. Once nucleation occurs, the remaining super-saturation can be relieved through condensation and fast particle growth (coalescence/coagulation). At sufficient high temperature particle coalescence (sintering) is faster than coagulation and spherical particles are formed. At lower temperatures, where sintering is negligibly slow loose agglomerates are formed. In order to prepare small particles it is necessary to create a high degree of supersaturation, thereby inducing the formation of a high nucleation density and then immediately quench the particle growth. This occurs rapidly (in the millisecond to second regime) in a relatively uncontrolled fashion, and leads itself to a continuous or quasi-continuous operation mode. This contrasts with colloidal synthesis of nanoparticles that are carried out in discrete batches under well-controlled conditions with batch times of hours to days.

Laser pyrolysis process is based on the resonance between the emission of a continuous wave (*cw*) $CO_2$ laser and the infrared adsorption band of a precursor or a component present in the incoming reactant stream [33], and the subsequent transfer of energy to non laser-active molecules. There is a broad range of available materials that absorb at 10.6 μm (0.12 eV). These can be broadly categorized as: i) precursors which directly produce the desired materials upon decomposition or chemical reactions following laser photolysis or pyrolysis,e. g. silane ($SiH_4$) to produce silicon nanoparticles [34] ii) sensitizers that only absorb and transfer energy to heat/decompose reactants without producing products and or participating in the reaction, e.g.$SF_6$ to decompose iron carbonyl for Fe nanoparticles synthesis [35] and iii) species that have the role of absorbing, decomposing and reacting to assist decomposition of precursor, e.g. ethylene in the presence of oxygen to produce vanadium oxide from vanadium oxy-trichloride vapor [36]. The high power of the $CO_2$ laser induces the sequential absorption of several IR photons in the same molecule, followed by assisted energy pooling leading to a rapid increase in the average temperature in the gas through vibration-translation energy transfer process [37].

In contrast to other vapor-phase synthesis methods, laser pyrolysis displays important advantages which permits highly localized and rapid heating (leading to rapid nucleation) in a volume that can be limited to a few hundred $mm^3$, followed by fast quenching of the particle growth (in a few ms). As a result, small nanoparticles are formed in the hot region. However, an unavoidable disadvantage is going along with this method. Agglomeration of the particles occurs after leaving the high temperature region since coalescence becomes much slower than coagulation (sintering).

*Experimental Method.* In a typical laser pyrolysis reactor configuration as shown schematically in Figure 15.2, the process of laser pyrolysis shown schematically in Figure 15.1, the continuous wave (*cw*) 10.6 micron wavelength of the IR $CO_2$ laser is passed through a reactor to intersect an orthogonally flowing reactant stream fed through a nozzle, to form a well-defined laser reaction zone (LRZ). An inert gas flows through the outer tube with the purpose of confining and cooling the particles. The chemical precursors can be either in gas or liquid phase, being the former the preferred option. The use of liquid precursors is made possible by bubbling the inert gas, or one of the gas phase reactants, through a flask containing the liquid precursor to carry out the vapor into the chamber. After leaving the hot reaction zone, the produced particles are driven by the gas flow into a trap; most often is a solid filter of cellulose. Recent works have also reported the direct collection of the freshly nucleated particles into a set of two bubbler vessels containing liquid media in order to reduce the degree of agglomeration [38]. The process generally operates under constant pressure governed by an electro valve. Typical cell pressures are in the range of 100-700 mbar [39].

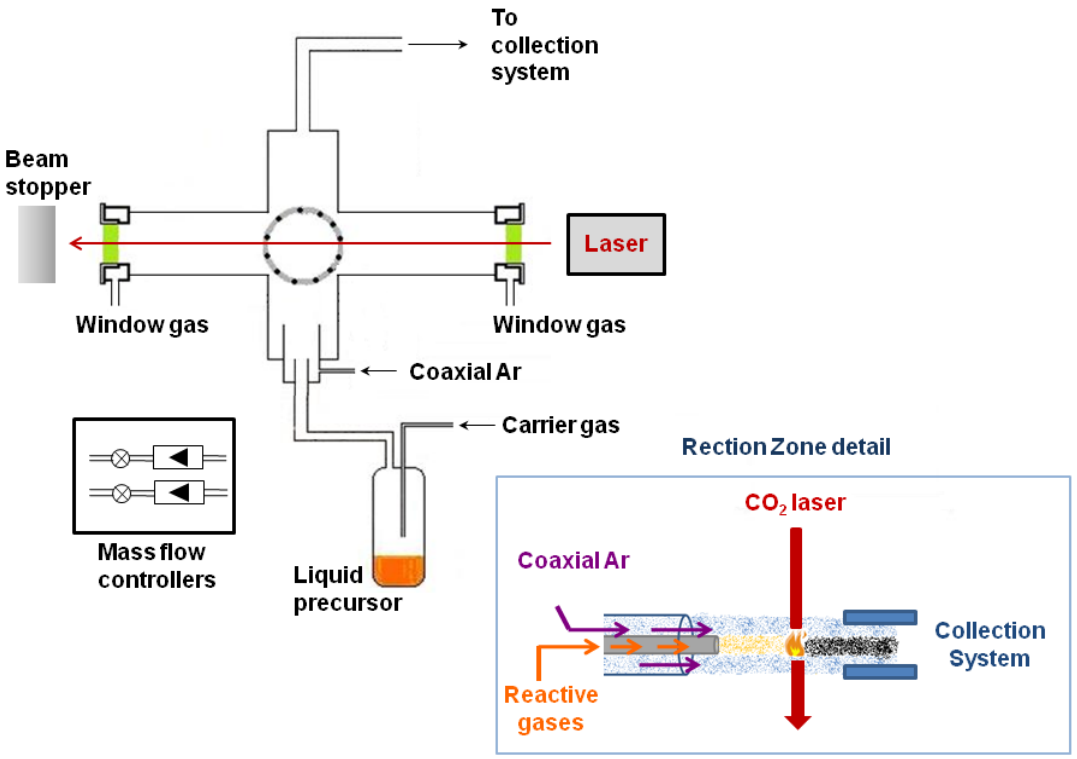


**FIGURE 15.2**
Schematic representation of the Laser pyrolysis device and detail of the reaction area where the IR laser interacts with the gas reactants

## Microfluidics for nanoparticles production

### Synthesis methods in microfluidics: approaches to tune monodispersity

Chemical reactions based on wet-chemistry are by far the most widely used method for the synthesis of nanoparticles in both bulk solutions and microfluidics[40]. Two or more reactants are brought together and reacted at the proper temperature and pressure conditions. Nanoparticles synthesis can generally be classified into two categories based on their flow types: continuous flow (single-phase flow) systems and segmented flow (multi-phase flow) systems[11]. The microreactors that are used in continuous flow-based systems include capillary tubes, coaxial flow microreactors, and 2D micromixing based reactors, and those used in segmented flow systems include gas-liquid segmented microfluidic reactors and liquid-liquid segmented or droplet-based microreactors. The droplet based microreactors are further classified into single-emulsion based, double-emulsion based and coalescence based reactors[41].

In continuous flow systems, the reagents are mixed by passive mixing, increasing the contact area between the mixing species so that the species are folded multiple times as they flow along the mixing channel. But, reagents are usually allowed to react in microchannels under diffusion-based laminar flow conditions. Nanoparticle quality is determines by several factors, such as reaction time,

temperature, efficiency of mixing and the concentration of the reagents. Both, laminar flow conditions and parabolic velocity profile control the diffusive mixing and residence time distribution (RTD) of reagents along the microflow system. If mixing time is high, the RTD is wide and thus nanoparticles with a wide particles size distribution are obtained[42]. Segmented flow systems are used to overcome continuous flow drawbacks. The reagents are mixed by active mixing, which utilizes segmentation to improve mixing[43]. Liquid–liquid or gas–liquid segmented flow, which is typically formed by creating discrete microdroplets in a second immiscible phase within the microchannel, improve the mixing because of the recirculation within the segments. Gas–liquid segmented flow reactors are attractive due to the simple separation process of the gas from the liquid once the nanoparticles are produced and flow to the reactor outlet. Then, liquid segmentation enhances reactant mixing, promoting a narrow RTD and reducing the nanoparticle size distribution[40]. However, there are some limitations arising from the requirement to find suitable fluids (reacting fluid/carrying fluid) that should be non-miscible over all the range of experimental conditions (pressure, Temperature, pH, etc.)[2].

In addition, further phase separation downstream are needed in order to separate the nanoparticle stream, which can be addressed through the use of phase separator[44] (see figure 15.3-a). The narrowness of the nanoparticle size distribution is commonly attributed to the reduced dispersion associated with segmented flows. But, recently, Sebastian et al.[10] demonstrated that it is the slip velocity between the two fluids and internal mixing in the continuous-phase slugs that govern the nature of the particle size distribution (see figure 15.1 b-e). In fact, the difference in the physical properties of the two phases and the inlet flow rates ultimately control the particle growth. It is then necessary a careful choice of continuous and dispersed phases to control the nanoparticle size and size distribution[10].

During the synthesis process a succession of processes occur simultaneously: nucleation, growth, coarsening, and/or agglomeration. The properties of nanoparticles directly depend on the phenomena which occur during these steps. For instance, if the nucleation-growth rate is faster than the mixing rate, poly-disperse nanoparticles are obtained. Microfluidic systems, generally defined as reactors having micrometer length scale fabricated by microtechnology and precision engineering, exhibit significantly enhanced control over each single process independently[40]. Edel et al.[46] demonstrated that it is possible to achieve rapid and controllable mixing via diffusion mediated transport. Monodisperse semiconductor nanoparticles were obtained because the microfluidic system enabled to control of both nucleation and particle growth.

In contrast, in conventional reactors mixing is driven by convective processes and the heterogenous mixing promotes nanoparticle agglomeration and widens particle-size distribution. These facts imply that recrystallisations[46] or size classification process[3] are required to get monodisperse nanoparticles, which made not feasible the production of this type of nanomaterials. An elegant and engineered-sophisticated microflow system was designed by Jensen group in order to produce high-quality phosphide nanocrystals in as little as 2 minutes[45]. A continuous three-stage silicon-based microfluidic system was arranged to tune reaction conditions in the mixing, aging, and growth steps (see figure 15.3-f).

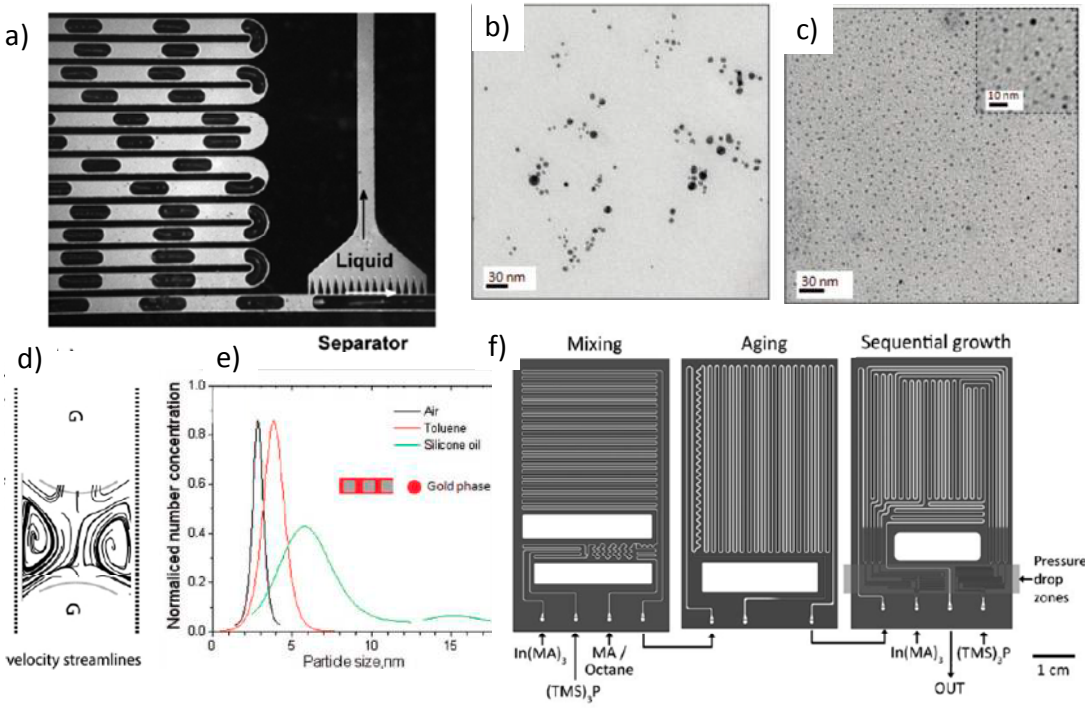


**FIGURE 15.3**
a) Segmented gas–liquid flow with the capillary separator integrated at the end. Reprinted with permission from ref. [42]; TEM image of gold NPs synthesized at in a hydrophilic reactor: (b) silicone oil−aqueous segmented flow, (c) air−aqueous segmented flow. d) velocity streamlines in a liquid slug (e) Particle size distribution diagram from AuNPs gas/liquid−aqueous segmented flow. Reprinted with permission from ref.[10]; f) Three-stage high-temperature and high-pressure microfluidic system with a mixing stage, an aging stage, and a sequential injection microreactor with six additional injection channels. Reprinted with permission from ref. [45]

On the other hand, micromixers enable to tune the mixing time to promote the production of monodisperse distribution of nanoparticles. By splitting reagents streams into a series n-substreams of similar width, mixing times decrease by a factor $n^2$, as the diffusion time is proportional to the diffusion distance[46] (see Figure 15.1e-f). Active mixing schemes, where it is applied external forces, improve the mixing performance by accelerating the diffusion process. This type of mixing is implemented by incorporating some form of mechanical transducer within the microfluidic device using microfabrication techniques[47]. Active micromixers typically use acoustic/ultrasonic, dielectrophoretic, electrokinetic time-pulse, pressure perturbation, electro-hydrodynamic, magnetic or thermal techniques to enhance the mixing performance. Micromixers with acoustic/ultrasonic actuation integrate a piezoelectric material, which after applying an external electrical field generates a strong acoustic streaming effect, enhancing species mixing within the channel. In dielectrophoretic force assisted micromixers, the electrical field generates a dipole moment on the molecules and the interaction between the induced dipole charges and the electrical field generates a net force which drives the particles either towards or away from the electrode[48]. The resulting chaotic motion leads to a rapid and efficient mixing effect[49]. On the other hand, electrokinetic time-pulsed microfluidic mixers apply an electrokinetic driving force to transport the sample fluids while simultaneously inducing periodic perturbations in the flow field.[47] Using this type of micromixers enable to achieve efficiencies

of up to 95% [47].The mixing in pressure perturbation mixers is generated by velocity pulsing within the fluid streams [50]. Electro-hydrodynamic micromixing is based on applying an electrical field perpendicular to the interface of fluids with different electrical properties. Applying the proper voltage and frequency to the electrodes, a satisfactory mixing performance could be achieved after less than 0.1 sec over a short mixing distance[51]. Regarding magneto-hydrodynamic flow effect micromixers, the coupling of DC or AC electrical and magnetic fields generate Lorentz forces which induce the stretching and folding of the fluid[52]. These forces enable the reagents mixing within several seconds[47].

To avoid complicated microfabrication processes and decrease the cost and complexity involved in using active micromixers, a generation of passive micromixers are used by microfluidic community. Passive micromixers neither contain moving parts nor require energy input other than the pressure head used to drive the fluid flows at a constant rate[47]. Consequently, the maintenance of passive micromixers is cheaper that in active ones. Mixing in passive micromixers is performed by the chaotic advection effects generated by manipulating the laminar flow within the microchannels or by enhancing molecular diffusion by increasing the contact area and contact time between the different mixing species. To promote the mixing of reagents and then the formation of monodisperse nanoparticles, several arrangements in micrchannels design have been proposed: intersecting channels, 3D serpentine structures, embedded barriers, slanted wells, and twisted channels[47]. Micromixers with intersecting channels can be used to split, rearrange and combine component streams to enhance mixing by shear stress[53, 54]. In zigzag microchannels, the dimension of the periodic zigzag unit is important to achieve a good mixing (Figure 15.3-f). The mixing efficiency increases from 65% to 83.8% as the geometry ratio s/w was increased from 1 to 8 (where s and w are the periodic length and channel width, respectively). But the mixing efficiency decrease at higher s/w ratios, which implies that there is an optimal zigzag geometry[55].

***Microfluidic synthesis of inorganic nanomaterials***

During the last years, there has been increasing interest in the synthesis of inorganic nanomaterials by using microfluidic methods. Microfluidics solve some of the challenges in reaction engineering[3], and so, there are a wide variety of inorganic nanoparticle synthesis reported[2, 11, 40, 56]. The main questions addressed relate to the control of the size and shape of the nanoparticles, being considered microfluidics as a possible technology to allow the investigation and the control of nanoparticle synthesis. The synthesis of inorganic nanomaterias can be classified according to the type of material as: metal, metal oxides, semiconductors, nanocomposites and other type of nanomaterias such as zeolites.

*Metal Nanoparticles.* Metal nanoparticles have attracted great interest due to their interesting optical, electronic, and thermal properties in fields such as electrical and nonlinear optical devices, dielectric materials bioimaging, optical hyperthermia, catalysis and electronics. Generally, metal nanoparticles are prepared by reducing the corresponding metal ions precursor with a reducing agent in the presence of stabilizing ligands. A number of ligands and surfactants systems have been used to stabilize the synthesized particles and minimize agglomeration and deposition on the walls of the microfluidic systems. Wagner et al.[57] reported the synthesis of Au nanoparticles using continuous-flow microreactor by reducing the gold precursor $HAuCl_4$ by ascorbic acid in the presence of PVP as stabilizing agent. Several parameters, such as the pH, flow rate and reagent concentrations were screened to tune the nanoparticle properties. This microfluidic device reduced twice the gold nanoparticles size distribution width as that obtained in a conventional synthesis. To prevent the

fouling or clogging of the reactor, the microchannel surface was chemically modified. The variation of residence time tested did not affect considerably the particle size, but the use of a strong reducing agent such as $NaBH_4$ decrease the particle size. These facts are consistent with a fast kinetic nucleation and growth reaction. Cabeza et al.[10] reported the controlled synthesis of Au nanoparticles, obtained using $NaBH_4$ as reducing agent, by air segmentation of the reactive microflows within the time scale of 10 s. Nucleation and growth of the nanoparticles take place inside the liquid slugs and benefit from the mixing characteristics of the two-phase flow. The particle size distribution was sensitive to the segmentation fluid as well as the residence time. These facts show that microfluidic reactors are the proper technology in reactions where the reaction time is short, since the mixing time must be shorter than the reaction time. Gomez et al.[58] recently reported the synthesis of hollow gold nanoparticles with interesting properties as optical probes for optical hyperthermia. These nanoparticles were obtained using a multi-step microfluidic reactor. The proper selection of synthesis parameters enabled the growth of these plasmonic nanoparticles, but also the functionalization with a biocompatible ligand and sterilization for further use in any biomedical application. Silver nanoparticle under 5 nm size could be obtained following the same approach[59].

Microfluidics not only allows tuning the nanoparticle size, but also the shape. Microfluidic continuous-flow synthesis of rod-shaped gold and silver nanoparticles[60] were produced just by adapting the conventional method reported in batch reactors. Conventionally, the method is based on the growth of metal nanorods from spherical metal seed crystals in an aqueous growth solution containing the $HAuCl_4$ or $AgNO_3$ precursors, a soft reducing agent, such as ascorbic acid, and a surfactant molecule, such as cetyltrimethylammonium bromide (CTAB). The online optical monitoring of the nanoparticles obtained in continuous flow allow to assure the rod-shape particle along the time[60]. A novel approach to produce gold nanorods was based in segmented flow[61]. Gold nanoparticle seeds and growth reagents were dispensed into monodisperse picoliter droplets .The confinement within small droplets prevented the contact between the growing nanocrystals and the microchannel walls, avoiding the reactor fouling. Nevertheless both approaches use a very toxic ligand (CTAB) to cap the nanorod surface and direct the anisotropic growth, which means that these nanoparticles could not be applied in biomedical applications without the surface modifications. Sebastian et al. produced gold nanorods in a continuous microflow reactor but using a novel method where the gold seeds were produced in-situ and afterwards they were grown into gold nanorods. Furthermore, the gold nanorods were capped with a compatible ligand (lysine), assuring a direct application in any biomedical application without further modification. Knauer et al.[62] synthesized high quality Ag nanoprisms in a two-step segmented flow process by chemical reduction of $AgNO_3$. In the first step, homogeneous Ag seed nanoparticles with average diameter of approximately 4 nm were prepared. In the second step, the growth of Ag nanoprisms was carried out within microfluidic segments by reduction of $AgNO_3$ on the non-capped surfaces. The edge length of the synthesized Ag nanoprisms was tuned to be between 35 - 180 nm ranges, just by adjusting the Ag seeds concentration of the seed particles. Copper nanoparticles were also obtained using a microfluidic reactor[63]. After comparing the nanoparticles obtained by both the conventional batch and the microfluidic processes, the copper nanoparticles formed in microfluidic devices were smaller (8.9 nm vs. 22.5 nm) and had a narrower size distribution, as well as an improved stability versus oxidation.

*Metal Oxide Nanoparticles.* Metal Oxide nanoparticles are widely used because their interesting applications as sensors, photocatalysts and luminescent materials and described. They can be obtained through several well-known procedures such as sol-gel or redox reactions. Magnetic nanoparticles are finding increasing application in areas comprising biomedical imaging, labeling, bio-sensing and

diagnosis, as well as drug delivery. For biological or biomedical applications, the particle size, nature of surface coatings, as well as the lack of aggregation is important to determine the determining application scope[40]. Superparamagnetic iron oxide nanoparticles have been synthesized using a stable passively-driven capillary-based droplet reactor, where the precursors ($FeCl_2$/$FeCl_3$/dextran and $NH_4OH$) were segmented by octadecene as carrier fluid[64]. The particles obtained were 3.6 nm in particle size, with a narrow size distribution. They were also found to be very stable and remained non-aggregated.

A gas-liquid segmented reactor was used to synthesize silica nanoparticles through the Stöber process[65]. The advantage of using gas in spite of liquid, as inert carrier, is that it can be inert and easily added or removed from the system[2]. A solution of tetraethyl ortho silicate (TEOS) in ethanol was contacted and premixed with an ammonium hydroxide solution. The segmentation of the flowing reacting medium was achieved by the injection of nitrogen as inert gas. Similar results were obtained by Gomez et al., using a passive micromixer instead of a segmented flow reactor[66]. Nevertheless, both type of reactors improve the reproducibility and size distribution obtained using the conventional batch process. Titania nanorods have also been synthesized in segmented flow microreactor. Nevertheless the carrier was not inert and, in this case, the reaction occurred at the interface between two liquids segments where the precursors were dispersed[67]. ZnO nanoparticles were prepared by micro segmented flow synthesis in tubular reactor[68]. The synthesis was carried out using a multi-step micro-continuous-flow process. It was observed that the particle size and optical absorption strongly dependent on the water content in the final mixture solution.

*Semiconductors*. Semiconductor nanoparticles have unique optical and electronic properties, and then, can be used in applications such as sensing and imaging. The physical properties of these nanoparticles are strongly related to their physical size and shape. Semiconductor materials have gained the earliest interest for microfluidic synthesis. Binary semiconductor compounds such as CdS, CdSe, and ZnS, were the first nanoparticles synthesized in a microfluidic system[46]. Conventional macroscale generation of semiconductor nanoparticles has some limitations and the particle size distributions are usually large and need post treatment to extract the desired particle size. Then, microfluidic systems have been proposed as an alternative synthetic approach to control nanocrystal growth, and the corresponding optical properties. The synthesis procedure to grow semiconductor nanoparticles involves the injection of a liquid precursor into a hot bulk liquid, followed by growth at a lower temperature in the presence of stabilizing surfactants, which enable the size and shape control. The exquisite temperature control required to achieve a fine particle size distribution makes microfluidics systems as the most appropriate tool of synthesis since an excellent mixing and heat transfer can be achieved. A variety of semiconductor nanomaterial have been synthesized using both continuous flow [69]and segmented flow[70] microreactors, incorporating microheater and micromixing units. A laminar microfabricated mixer was used in the first reported microfluidic procedure[46]. A wide variety of nanoparticle sizes were obtained just by tuning the residence time of reagents, obtaining better results than in the conventional approach. Since this work was published, a numerous list of publications have deal with the synthesis of semiconductor nanoparticle by the microfluidic approach[2]. Initial studies in continuous synthesis of semiconductor nanomaterials were performed at atmospheric pressure using a single phase laminar flow capillary reactors[71]. Although these devices have the advantages that are commercially available and do not requiring any microfabrication procedure, as well as their access is feasible for online characterization[72], they suffer from undesired performance if high viscous solutions are used. High viscosity leads to slow mixing, broadening the residence time distributions and then promoting the production of nanoparticles with a heterogeneous size distribution[2, 71].

Application of segmented flows for continuous synthesis overcomes these shortcomings by narrowing the RTD. CdSe nanoparticles has been synthesized in both liquid–gas[70], and liquid–liquid segmented flows[73]. Comparing the results obtained in both continuous-flow and segmented-flow methods, it was observed that the enhanced mixing and narrow residence time distribution characteristic of the segmented-flow reactor resulted in a significant improvement of the size distribution and reaction yield, being more convenient for short residence times experiments[70]. Hung et al.[74] proposed a microfluidic device that was based in the fluid segmentation, but the segments were fused under a velocity gradient in an expansion chamber. The synthesis of nanomaterials at high temperature is a challenge, and outgassing and clogging are usual problems encountered during the synthesis within microreactors. These drawbacks can be faced by the selection of appropriate chemical reagents[71]. A novel approach in the synthesis of CdSe nanoparticles at high pressures and temperatures in a continuous microfluidic system is using a supercritical fluid as a solvent[75]. The synthesis in supercritical conditions resulted in a decrease of 2% in the size distribution of the CdSe nanoparticles due to a decrease of the residence time distribution caused by its lower viscosity compared to non supercritical conditions. Also, the use of supercritical fluid promotes a higher supersaturation, which led to produce a larger number of nuclei, thus narrowing the size distribution of nanoparticles. The presence of temperature gradients in a two-temperature approach microfluidic systems improve the control over the nucleation and growth of the nanoparticles, decreasing the size distribution and enables a superior kinetic control on growth process[69]. CdSe nucleation was induced in the high-temperature zone and then, the nuclei were grown at the low-temperature zone. A further development in semiconductor nanoparticles synthesis was performed by Baek et al.[45]. They combine the advantages of both temperature gradient microfluidic systems and supercritical fluids to create a continuous three-stage microfluidic system that separates the mixing, aging, and subsequent injection stages of InP nanocrystal synthesis. The microfluidic system operates at high temperature and high pressure enabling the use of solvents in the supercritical regime to promote high diffusivity, which results in the production of high-quality InP nanocrystals in a time scale as short as 2 minutes. The quality and stability of semiconductor nanoparticles such as CdS and CdSe can be improved by covering them with a thin shell of another semiconductor nanomaterial. Microfluidic systems have emerged as a feasible tool to control the coating on semiconductor nanocrystals[76].

*Nanocomposites.* The flexibility in designing microfluidic systems and the possibility to add reagents at different reaction stages make microfluidic systems suitable for generation of complexly structured materials. Multi-step microfluidic systems ease the synthesis of complex onion-type nanoparticles such as double shell nanoparticles. Au/Ag/Au double shell nanoparticles were prepared using a two-step micro microfluidic system[77]. The synthesis was based on the reduction of $HAuCl_4$ and $AgNO_3$ at the surface of seed particles by ascorbic acid, using a segmented flow microreactor. This approach led to nanoparticles with smaller size and narrower size distribution than in the batch synthesis, due to effective mixing inside the micro segments. Sequential addition of reagents is a clever strategy reported is to create core-shell $SiO_2$@$TiO_2$ nanoparticles and tune the thickness of the shell on demand [43]. Gomez et al.[58] recently reported the synthesis of hollow gold nanoparticles obtained in a multi-addition reactor, where Co nanoparticles were first synthesized as templates of Au hollow nanoparticles. After gold precursor addition to replace Au by Co, nanoparticles were functionalized with a biocompatible ligand (PEG) and sterilized. A successive microfluidic approach to create hierarchical catalyst nanostructures consisting of metal-decorated nanoparticles that are assembled into porous microparticles was developed by Lee et al.[78]. First, using a silicon-etched microreactor, tiny platinum nanoparticles were grown and immobilized onto iron oxide/silica core–shell nanospheres. Afterwards, the Pt-decorated silica nanospheres were assembled to form micron-sized particles by

using emulsion templates generated with a microfluidic drop generator. These nanostructures were reported to show an excellent catalytic activity. Combining organic and inorganic materials synthesis strategies in microfluidics opens opportunities for realizing nanocomposite microparticles made of organic materials and incorporating inorganic. A new strategy to generate a wide variety of multifunctional nanostructures using a fast procedure was developed by Zhao et al.[79]. They prepared quantum dot barcode particles by polymerizing double-emulsion droplets prepared in capillary microfluidic devices. The resultant barcode particles were composed of stable quantum dots with different optical properties, surrounded by hydrogel shells. They also could fabricated anisotropic magnetic barcode particles with two separate cores, one which enables optical encoding and other magnetic separation. Another method based on solvent evaporation, was used to prepare core shell CdSe@ZnS semiconductor nanoparticles embedded in PLGA microcapsules[80].

*Other Materials.* The synthesis of nanomaterials with a higly crystalline structure, such as zeolites, is problematic since it is require a long reaction time that typically lasts up to 1-2 days, even under hydrothermal conditions with high autogenous pressures and high temperature in discontinuous batch processes[81]. Hoang et al.[82] reported a droplet- and ionic liquid assisted microfluidic synthesis approach, which takes full advantage of both ionic liquids and droplet-assisted microreaction systems, for an ultrafast, mild, and continuous synthesis of zeolite ZSM-5. Using a T-junction they dispersed a precursor solution into a segmented flow. The solvent used for the droplet phase consisted of a mixture of water and an ionic liquid. The presence of the ionic liquid was necessary to prevent reactor clogging and provide water molecules to the reactive medium. Authors found that crystalline ZSM-5 could be produced in 15 minutes, which was much less than the several hours in batch synthesis. A water-liquid paraffin two-phase segmented microfluidic reactor was also used to produce ultrafine zeolite A crystals with narrow particle size distribution[83, 84]. Some inorganic crystalline nanomaterials, such as hydroxyapatite, were also synthesized in microfluidic systems[85]. Nano-precipitation of hydroxyapatite was carried out in ultrasonic microreactors. The as-prepared nanoparticles were more crystalline and with a lower carbonate contamination than the nanoparticles obtained in batch approach.

***Microfluidic synthesis of polymeric nanomaterials***

The production of organic nanomaterials from new polymers to biomaterials such liposomes, has attracted increasing interest in material engineers. Nanomedicine is the application of nanotechnology to medicine, which involves the use of engineered nanomaterials for therapy and diagnosis of major diseases such as cancer, cardiovascular and infectious diseases[86]. The first generation of nanoparticles with applications in medicine dates back to 1965, when nanoliposomes were synthesized for a wide range of biological and pharmaceutical applications. Liposomes were developed to deliver their cargo to cells: genes, drugs or other therapeutic agents and contrast agents. While a homogenous size distribution is critical to assure a controlled drug dosage, liposome size also ultimately influences the detection and clearance rate by the complement system[87]. The production of liposome formulations with a defined size and little size variation is challenging. There are different techniques to produce nanoliposomes, such as injection, sonication or membrane extrusion. But liposome populations produced from those different techniques are not very efficient to control the variability in terms of mean size and population homogeneity. Microfluidic systems have been used in the production of organic nanostructures because of their excellent properties to control size and shape of nanoparticles in a reproducible fashion. Electro-formation of liposomes in microchannels resulted in giant unilamellar liposomes with a mean liposome diameter of about 12 □m[88]. A different approach was based on a fluidic crossflow ethanol injection method to produce homogenous liposome populations[89]. Liposomes

form at the miscible buffer/ethanol interface, varying the particle size between 200 nm and 500 nm. The microfluidic cross flow injection method helps to achieve a better control and reproducibility that the manual procedure. The approach which allows decreasing the size of nanoliposomes under 300 nm using the hydrodynamic focusing was developed by Jahn et al.[90]. Adjusting the volumetric flow of different reagents provides a tool to modify the average liposome size and size distributions.

Over the past two decades, a number of microfluidic approaches have been developed and widely applied for making single droplets, and droplet-in-droplet, also known as double emulsions. The existing microfluidic approaches for making single emulsions involve the injection of one microflow (the dispersed phase) into another immiscible or partially immiscible liquid phase (the continuous phase), and droplets are sheared off at the junction where the two phases meet[91]. On the other hand, double emulsions are typically generated in a two-step process by first forming the inner droplets, which are further encapsulated in a second emulsification step[91]. Regarding the solvent polarity and microfluidic system wettability, two-stage microfluidic devices have been widely used in generating either Oil/Water/Oil[92] or Water/Oil/Water[93] double emulsions. Polymerization reaction in droplets[94] or at interfaces combined with the ability of microfluidic systems to manipulate nanoliter volumes of liquid, and control mixing and reaction precisely have led to the synthesis of polymer particles[95]. Photopolymerization offers a flexible approach to form particles in microfluidic systems. Two key reagents, monomers and activators, are mixed inside droplets and are exposed to near ultra violet light to promote the curing and initiate the formation of the final polymer particle shape[96]. Combination of photopolimerization and multiple laminar co-flowing liquids enable the formation of Janus nanoparticle and complex structures. For instance, the manipulation of microfluids with a stop flow approach enabled the formation of polymer nanoparticles with a controlled shape and functionality[97]. Other microfluidic techniques for producing polymer particles without the addition of activators, which sometimes are not proper for the further applications, are based on the precipitation. These methods are based on solvent removal and the addition of an antisolvent. The main limitation of these techniques is finding a suitable solute–solvent system which fulfills the evaporation and solubility requirements[2]. PLGA–PEG copolymer nanoparticles have been obtained by flow focusing, using acetonitrile and water solutions as solvent and antisolvents, respectively[98].

## Synthesis of nanoparticles by laser pyrolysis

Laser pyrolysis as a synthesizing method has been applied to the fabrication of a large variety of compositions (Figure 15.4). The literature reports the possibility to produce a broad spectrum of materials including carbides (SiC, TiC), nitrides ($Si_3N_4$, BN, FeN…), oxides ($TiO_2$, ZnO, $Fe_2O_3$) or composites powders (Si/C/N, Li/Mn/O, Fe/C/N…) but also single-element nanostructures such as carbons (Fullerenes, diamonds, and carbon black), metallic iron or silicon. This section briefly presents the capabilities of laser pyrolysis processing and outlines the level of control to design functional nanomaterials. The first part overviews multiple examples related with the synthesis of metal oxides and the second part focuses on single-element nanoparticles.

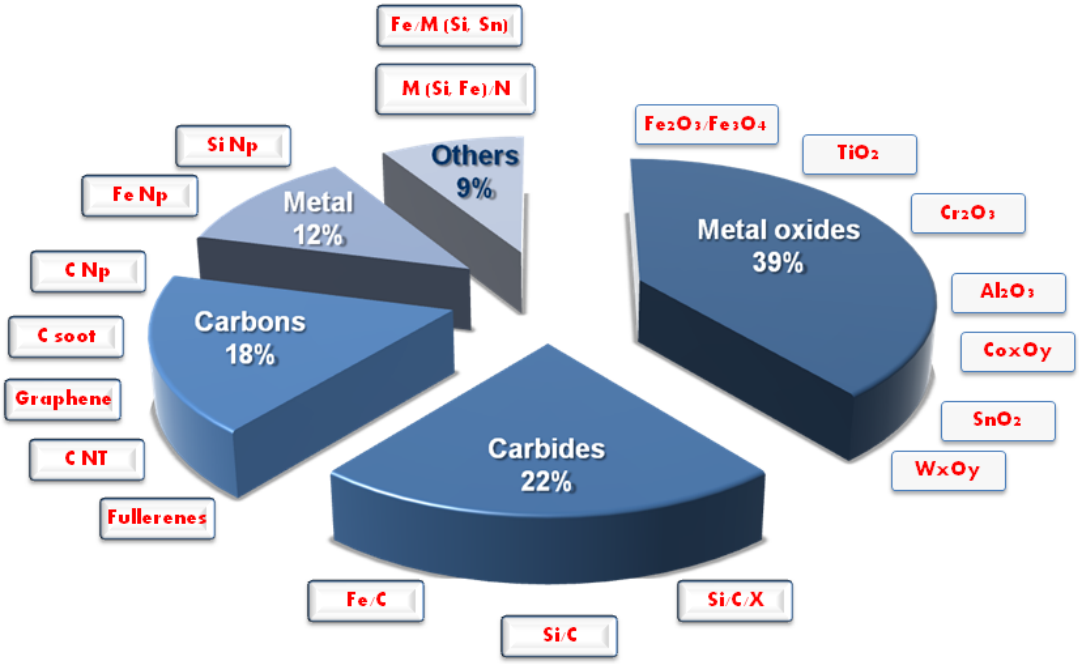


**FIGURE 15.4**
Scope of the laser pyrolysis technique regarding to the large variety of materials compositions that can be produced and the ratio expressed in fraction of 100

***Laser pyrolysis applied to the synthesis of metal oxides***

*Iron oxides.* The fabrication and characterization of nanosized magnetic particles are the subject of intense research motivated not only by their interesting properties, quite different from those of the corresponding bulk materials, but also from the point of view of their promising technological and/or biomedical applications, such as magnetic recording media, ferrofluids and soft magnetic materials [99]. Below a critical size, magnetic particles become single domain in contrast with the usual multidomain structure of the bulk magnetic materials and exhibit unique phenomena such as superparamagnetism [100] and quantum tunneling of the magnetization [101 102]. Fe and O form a number of phases, e. g. FeO (wustite); $Fe_3O_4$ (magnetite), $\alpha$-$Fe_2O_3$ (hematite), $\gamma$-$Fe_2O_3$ (maghemite), and $\varepsilon$-$Fe_2O_3$ [103]. The latter two phases are synthetic while remaining oxides occur in nature. The Fe-O phase diagram shows the predominance of the $Fe_2O_3$ stoichiometry for most temperature and pressure preparation conditions [104].

The continuous production and structural characterization of iron oxide nanoparticles, mainly $\gamma$-$Fe_2O_3$ phase, has been extensively reported since the application of laser pyrolysis in the thermal decomposition of metal carbonyl organometallic complexes [31]. Iron pentacarbonyl in particular exhibits attractive properties for conventional [105] and laser chemical vapor deposition CVD processes [106], i. e., sufficiently high vapor pressure and low activation energy for breaking the metal-CO bonds [31]. Previous reports [31, 107] indicate that, in the case of $Fe(CO)_5$ gas-phase decomposition, the rate-determining process is the first decarbonylation of the thermally excited $Fe(CO)_5$ into $Fe(CO)_4$ and CO; it has been observed [35] that further decarbonylation from $Fe(CO)_{5-m}$ (m= 1-4) to $Fe(CO)_{4-m}$ and CO proceeds rapidly

due to the weaker remaining bonds. The final products of the fast decarbonylation should be iron and carbon monoxide, but the decomposition yield will obviously depend on the reaction temperature, which in turn is determined by the irradiation parameters and the absorbance capacity of the reactants gases. In contrast, the negligible radiation absorption by the metal donor gas precursors ($Fe(CO)_5$) requires the addition of a reaction sensitizer, an energy transfer gas, which can either react or interfere, thus altering the expected reaction path. Due to their strong absorbance at 10.6 microns ethylene ($C_2H_4$) and sulfur hexafluoride ($SF_6$) are the most common sensitizers employed [108]. However, the absolute absorbance of $SF_6$ is much greater than that of ethylene in this range.

The absorptive capacities of the precursors is largely related to the sensitizer nature that in most cases determines the productivity rates, the chemical composition of the products obtained and also the particle morphology [108, 109] . Due to the higher temperatures involved when $SF_6$ is used as sensitizer, the nanopowder yield increases while a lower productivity is reached with $C_2H_4$ as sensitizer [108]. However, mainly because of the higher absorption cross-section of $SF_6$ at about 950 $cm^{-1}$ relative to $C_2H_4$, it is found that when using a high $SF_6$ flow rate, which leads to relatively high temperature in the reaction zone, F was present in the product nanoparticles, most likely as iron fluoride compounds [110]. Extraordinarily pure particles of $\gamma$-$Fe_2O_3$ smaller than 5 nm with different degree of crystallinity were synthesized from a nebulized isopropanol solution of $Fe(CO)_5$ in the presence of air [111-113]. However, the process provided low throughput, mainly because the energy coupling of the laser to the reactant mixture was achieved through a proper matching between the laser wavelength (10.60±0.05 μm) and the isopropanol band at 10.50±0.08 μm. Following this investigation, with the propose of increasing the reaction yield, Marteli et al. injected in the reactor chamber a mixture containing $Fe(CO)_5/NO_2$, using $SF_6$ as sensitizer [114]. $N_2O$ was used as an oxygen donor to obtain more reactive atomic oxygen instead of $O_2$ molecules and to favour iron oxidation. Depending on the experimental conditions they produced different iron-oxide phases. However, due to the high temperature reached in order to increase the reaction yield, the synthesis process led to the preferential formation of iron fluoride compounds.

The effect of process conditions on the structural and magnetic properties of maghemite nanoparticles produced by laser pyrolysis have been studied by Veintemillas-Verdaguer and co-workers [115]. They reported that the particle size depends on the oxygen content of the gas phase and is independent of the laser power [115]. One of the main problems of ultrasmall iron oxide nanoparticles is related to surface disorder[113, 116, 117], which has a direct impact on the particle's properties (i.e., the magnetic properties). In order to overcome this issue, Veintemillas-Verdaguer's group [118] has optimized a chemical protocol consisting of an acid treatment to improve the colloidal and magnetic properties of ultrasmall iron oxide nanoparticles prepared by laser pyrolysis via a reduction of the surface disorder. After acid treatment, the obtained particles presented smaller sizes, larger surface charge densities, and better colloid stability, which represent an enhancement in the colloidal properties and additionally, an enhancement of the saturation magnetization by 40 % with respect to that of the as-prepared sample. Morever, the exchange anisotropy field was significantly diminished, providing evidence of a reduction of the surface disorder.

Laser pyrolysis technology seems to be a good alternative for the production of magnetic NPs to be applied for Magnetic Resonance Imaging (MRI) as contrast agents with the advantage of being a continuous synthesis method. Biocompatible magnetic dispersions have been prepared from $\gamma$-$Fe_2O_3$ nanoparticles (5nm) synthesized by continuous laser pyrolysis of $Fe(CO)_5$ vapors [119-121]. Particles were collected directly from vapor phase onto filters. This allowed higher purity in the product. However, post treatment efforts are required to obtain dispersed nanoparticles into a liquid. The magnetic solid

was dispersed in a strong alkaline solution in the presence of dextran. The feasibility of these dispersions to be used as magnetic resonance imaging (MRI) contrast agents has been analyzed in terms of chemical structure, magnetic properties, 1H NMR relaxation times and biokinetic. Magnetic and relaxometric properties of the dispersions were of the same order of magnitude than those for commercial contrast agents produced by wet chemical methods. However, these dispersions injected intravenously in rats at standard doses showed a monoexponential blood clearance instead of a biexponential one, with a blood half-life of 771 min. Furthermore, an important enhancement of the image contrast was observed after the injection mainly located at the liver and the spleen of the rat. Recently, Marcu et al. have applied the laser pyrolysis-prepared iron oxide nanoparticles to investigated their cellular uptake and VB1 delivery to breast adenocarcinoma tumor cells [122]. They produced 8-10 nm magnetic nanoparticles from the pyrolysis of $Fe(CO)_5/C_2H_4$ and air mixtures and compared them with commercial pure iron oxide nanoparticles of 20 nm. The laser pyrolysis-produced nanoparticles were better internalized in the cytoplasm of MCF-7 tumor cells. They showed a lower action on cell adhesion/proliferation than the commercials ones, which is a convenient behavior for the use of NPs as drug delivery systems.

While the focus of this technique has been to reduce the primary particle size to below 30 nm, the problem of aggregation of nanopowders (Figure 15.5a) has not been adequately addressed [115]. Only few works oriented to improvement the particles dispersion are reported[110, 123]. The idea is to overcome the aggregation issue by collecting the iron-based nanoparticles directly into a solvent as an alternative to the standard collection systems previously used in laser pyrolysis systems [108]. Popovici et al. [123] achieved a selective particle collection mainly by the trapping of large particle aggregates into toluene prior to the collection filter. Nevertheless, most of the particles still remained as aggregates above 1μm in size. He et al. [110] reported better results in term of narrower size distributions. They obtained iron-based nanoparticles with 2–10 nm sizes containing $\alpha$-Fe and $Fe_3O_4$ phases directly collected into toluene solution containing stabilizing ligands. However, their particles showed a certain tendency to agglomeration and interparticle coalescence.
Martinez et al. [38, 39] recently addressed the main bottleneck in the synthesis of magnetic nanoparticles by laser pyrolysis. In order to circumvent the problem of agglomeration, the authors claim that not only is necessary to collected the nanoparticles into a liquid but also it is required the use of an appropriate solvent. They selected triethyleneglycol (TREG) due to its capacity as a capping agent and because has some key properties that hinders the aggregation of the particles. This strategy rendered a stable colloid suspension of well-dispersed ultrasmall iron oxide nanoparticles (< 3 nm) in a water-compatible solvent (Figure 15.5b). Therefore, this collection method constitutes a superior alternative not only regarding conventional filter-based collection, but also with respect to previous liquid collection results based on toluene or dextran. The efficiency of this collection approach based on the use of polyols can be explained in terms of the dynamics of the NPs formed in the reaction zone and entrained as part of the main gas stream. Using conventional dry collection filters, inter-particle collision of entrained NPs is favored by the nature of the filtration mechanism. In contrast, in the liquid collection system, a small fraction of NPs present in a gas bubble are collected over the bubble gas – liquid interphase and the likelihood of collisions with existing particles is prevented. Afterwards, the NPs are entrapped within the partially viscous liquid solvent through a hydrophilic coating that is able to stabilize them.

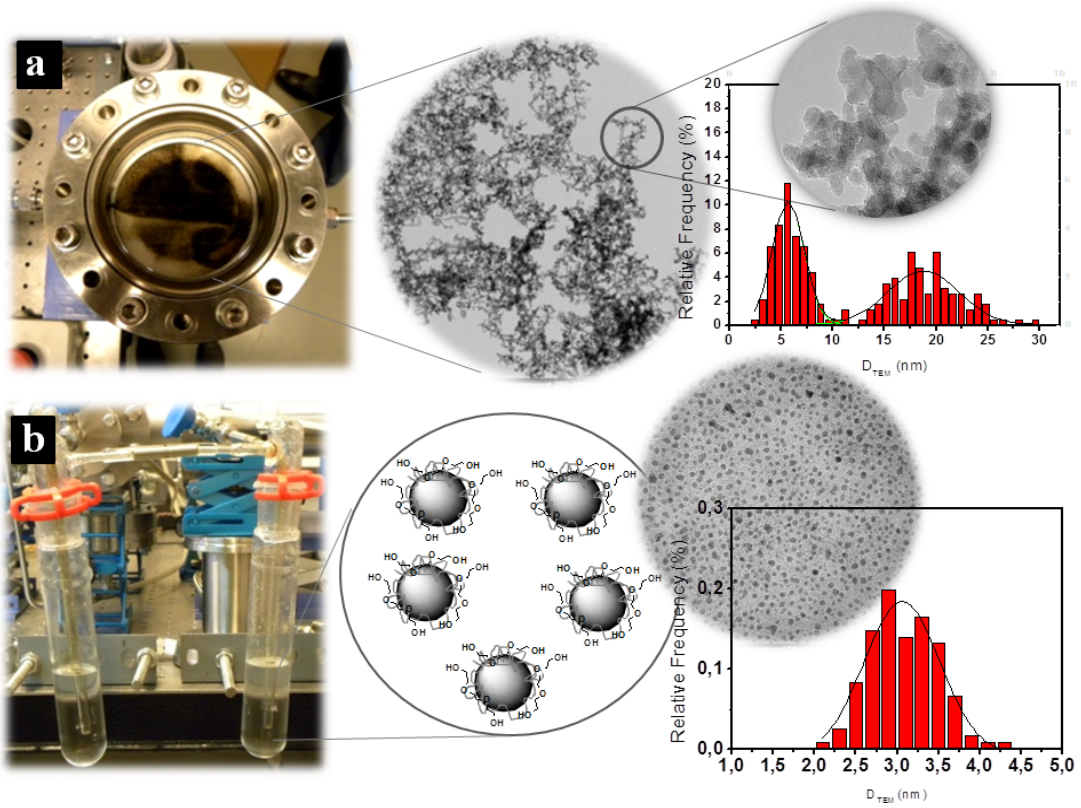


**FIGURE 15.5**
Magnetic nanoparticles of iron oxide prepared by laser pyrolysis and average particles size: (a) collected in a filter, (b) collected in liquid medium.

*Titanium oxides.* Titanium dioxide ($TiO_2$) is one of the most prominent oxide materials for industrial applications related to catalysis such as the selective reduction NOx in stationary sources [124, 125], the photocatalytic degradation of organic pollutants [126] or organic synthesis processes[127]. It is used as white pigment in painting, as part of photovoltaic devices [128] or electrochromic devices [129], sensors , as a food additive [130], in cosmetics [131] and as a potential tool in cancer treatment [132]. In $TiO_2$ materials, the so-called "quantum confinement" or "quantum size effect" is restricted to very low sizes, below 10 nm, due to their rather low exciton Bohr radii. A significant part of the potential novel chemical or physical applications needs to be carefully explored in the range of few nanometers[133, 134]. $TiO_2$ occurs in the nature in three different polymorphs which, in order of abundance are rutile, anatase and brookite. As an extended (bulk) system, rutile is the thermodynamic stable phase. When primary particle size is scaled down, a thermodynamic analysis of phase stability indices that surface free energy and stress contributions stabilize anatase below a certain size close to 15 nm [135 136].

Since 1987, laser pyrolysis technique has been used to synthesize $TiO_2$ nanoparticles [137]. Organic tetra-alkoxides titanium compounds [137, 138] such as titanium isopropoxide, butoxide or ethoxide are mainly employed as the Ti source, among them, titanium isopropoxide is the most widely used due to its higher volatility [139]. Ethylene and $SF_6$ have the role of reaction sensitizers for the absorption of the $CO_2$ laser irradiation wavelength. However, several advantages have been verified using $SF_6$ as sensitizer,

due to its about 20 times higher absorption coefficient for the P(20) laser line [139]. Early laser-induced processes were studied and developed for the synthesis either of pure $TiO_2$ powders, for use as a catalytic supports [138], [140-145] or directly as catalysts for example in the selective reduction of nitrogen oxides with ammonia [139]. In most of these works a post-calcination treatment was necessary to eliminate carbon contamination of nanopowders. In order to overcome this problem, Alexandrescu and co-workers reported for the first time the used of $TiCl_4$ as a precursor for the synthesis of titania by laser pyrolysis [146]. In the flow gas mixtures, oxidizers (like $NO_2$ and air) and sensitizers ($C_2H_4$) were also used. The results indicated the simultaneous presence of anatase and rutile phases, with prevalent anatase formation and suggested that the processing conditions have a strong influence on the structural properties of the material and in the anatase/rutile composition ratios [147]. This group also correlated the dependence of some major process variables, such as, the laser power and the oxidizer precursor flow with the obtained nanostructures [148]. Similar crystallographic features were found for the samples obtained at increasing laser power intensities. Likewise, crystallinity enhancement as well as a larger rutile fraction was also observed at a moderate increase in the flow rate of the oxidizing agent[149].

The new tendency in this field is oriented to the synthesis of dopped $TiO_2$ nanoparticles, for example iron [150] or carbon doped among others [151]. In addition, important research efforts have also been paid the synthesis of nitrogen-doped titanium dioxide [147, 152, 153]. Currently, this is an especially active field since the study of Asahi demonstrating, the appearance of a second optical threshold attributed to a $TiO_2$-xNx structure and correlated to an enhanced photocatalytic activity [154-156]. N. Herlin-Boime et al. are pioneers in this field. They synthesized TiOxNy by laser pyrolysis of titanium isopropoxide and $NH_3$ mixtures; ammonia was used as sensitizer and as nitrogen source [147]. To remove the C atoms, after the synthesis the samples were submitted to soft thermal treatment in air. They correlated the changes in electronic structure (N doped or pure $TiO_2$) with the evolution of UV absorption properties. Recently, they have investigated the use of nitrogen-doped $TiO_2$ electrode based on nanocrystals synthesized by laser pyrolysis for solid-state dye-sensitizer solar cells [157]. They demonstrated laser pyrolysis technology benefits from the synthesis of this material given its versatility for straightforward doping procedures. The influence of nitrogen doping was found to be beneficial on device performance, with a significant improvement of photocurrent compared to the pure $TiO_2$ device.

*Oxides systems containing Al, W, and Cr.* Due to the nanometric size of the constituent particles in the laser pyrolysis synthesized powders, this technique has also been tested on the synthesis of large variety of different oxides systems, such as $Al_2O_3$, $WO_3$ or $Cr_2O_3$.

Regarding the Al-O system, attention is mainly focused on the $Al_2O_3$ stoichiometry due to its importance as a catalyst component or absorbent and ceramic material in a multiple of industrial process. [158, 159]. There are seven $Al_2O_3$ polymorphs, although only four called $\alpha$, $\delta$, $\theta$ and $\gamma$ are typically involved in most of the industrial processes. The $\gamma$-$Al_2O_3$ is the nanostructures phase commonly obtained by most synthetic methods but also the $\alpha$-$Al_2O_3$ polymorph is synthesized having high surface area. The $\alpha$-$Al_2O_3$ structure is the bulk thermodynamically stable phase but $\gamma$-$Al_2O_3$ has a lower surface energy and becomes energetically stable at size bellow a point close to 10 nm [160]. Trimethylaluminium (TMA) is commonly used as a precursor in this method and $NO_2$ as oxygen donor. Ethylene is usually used as sensitizer to initiate and sustain the reaction due to the negligible radiation absorption of both components at the emission wavelength of the $CO_2$ laser. However, in the earlier attempts to produce $Al_2O_3$ nanopowders low production of $Al_2O_3$ was accompanied by a huge amount of free carbon formation [161]. Further efforts [150] made to increase the powder productivity also showed that any variation in the process parameters influence nor only the yields, but also the chemical composition of

the resulting powers, drastically changing their properties. Depending on the relative concentration of the precursors, the laser-induced reactions led either to a particle nitriding of the alumina-based powder or to the formation of aluminium oxycarbide [162].

Tungsten trioxide ($WO_3$) is known as a 'smart material', because it exhibits excellent electrochromic, photochromic and gasochromic properties. Nano-sized tungsten trioxide has been applied in many nano-photonic devices for applications such as photo-electro-chromic windows [163], sensor devices [164] and optical modulation devices [165]. Laser pyrolysis has been used for synthesizing nano-sized tungsten trioxide [166, 167]. Recently, it has been reported by Govender et al. [168] the production of multi-phase $WO_3$ and $WO_{3-x}$ (where x could vary between 0.1 and 0.3) nanostructures at varying laser wavelengths (9.22-10.82 mm) and power densities (17-110 W/cm$^2$). Tungsten ethoxide $W(OC_2H_5)_6$ was used as starting precursor and acetylene ($C_2H_2$) as sensitizer gas. Nanosized chromium (III) oxides powders have also been synthesized by laser-induced pyrolysis of chromyl chloride vapour. Kern and co-workers determined the optimal reaction conditions [169] and tested the powders as catalysts in technical processes, especially in the dehydration of isobutane to isobutene. They found that using argon as carrier gas, chromyl chloride was transformed into chromium (III) oxide with a good conversion rate and particle diameters of about 200 nm. Later on, Schramm's group [170] investigated the influence of the reaction parameters, for example, the pressure in the reaction chamber, on the mean particle diameter of the chromium (III) oxide powders and tried to get quantitative results. Small particles were obtained with lower pressure in the reaction chamber and a carrier gas with high thermal conductivity.

***Laser Pyrolysis applied to the synthesis of single-element nanoparticles***

Formation of single-element ultrafine particles has been also achieved by laser pyrolysis, being in most cases silicon or iron nanoparticles the mainly material produced. Only few works on laser pyrolysis synthesis referred to different metals nanoparticles have been reported. Swihart and co-workers [171] *in situ* synthesized superparamagnetic Ni (0) nanoparticles from $Ni(CO)_4$ .
In this section we refer the discussion to the laser pyrolysis process applied to the synthesis of silicon and carbon-based nanoparticles.

<u>*Silicon nanoparticles.*</u> Si and Si-based nanoparticles were the first to be produced by laser pyrolysis and probably the most widely investigated for two main reasons: (i) silane gas, a common precursor for Si radical formation, has a very high absorption capabilities for the emission line of an untuned, multimodal $CO_2$ laser (at 10.6 μm); (ii) the enormous importance of the photoluminescence properties [172] of Si and Si-based nanoparticles for a multitude of applications[173-176]. From the many possibilities to dissociate the precursor molecules, $CO_2$-laser-induced decomposition of $SiH_4$ in a gas flow reactor has been shown to be particularly useful for the production of ultraclean silicon particles in the nanometer size range as first shown more than 20 years ago [29]. It produces highly pure particles with controlled primary particle size and size distribution. Moreover, it is a continuous process that permits reasonable production rates. Several groups have synthesized silicon particles following similar approaches but without obtaining bright nanoparticles[177, 178]. As an exception to this trend, the work of Huisken and coworkers [179], reported the use of pulsed $CO_2$ laser pyrolysis of silane to obtain luminescent particles with low production yields. They also studied the effect of aging in air and surface etching with HF on the photoluminescence spectrum [172, 179-183] and concluded that efficient photoluminescence (PL) could be obtained for silicon nanoparticles smaller than 5 nm, with "properly passivated" surface to minimize the number of non-radiative recombination sites [172].

A significant contribution in this field was provided by Swihart and co-workers [34]. They produced macroscopic quantities (up to a few hundred milligrams in a few hours) of Si nanoparticles with an average diameter of about 5 nm and bright visible photoluminescence, using $SiH_4$ as silicon precursor and $SF_6$ as sensitizer. Availability of high quantities of particles allowed them the study of their surface functionalization [184]. However, this work offered a major disadvantage. Chemical etching with HF-$HNO_3$ was necessary in order to get particles smaller than 10 nm from the raw pyrolytic powders. Modeling of the synthesis of silicon nanoparticles by laser pyrolysisi were carried out by P.E. Nunccio and S. Martelli [185]. A sectional coagulation model was used to predict the evolution of the silicon nanoparticles in terms of both average particle size and average crystallite size. Recently, research in this field is focused in novel application of the laser-synthesized silicon nanoparticles. Reynaud's group [186, 187] applied the silicon nanopartiles produced by laser pyrolysis in photovoltaic solar cells or as biomarkers[173, 174, 176]. However, it should be emphasized the contribution of Swihart's group in the field of nanomedicine. They prepared Si nanocrystals following well-established laser pyrolysis procedures [34, 184] and studied their biological application. The biocompatible silicon nanocrystals obtained [173] were applied for multimode imaging *in vivo* Targeted Cancer Imaging [174].

*Carbonaceous nanomaterials.* Carbon-based nanomaterials has become of great interest lately, due to the great versatility of carbon as an element and the several ways in which it may combine, acquiring unique specific properties and becoming an interesting material for multiple applications. Carbonaceous materials exist in a wide variety of forms including carbon, graphite, diamond, highly oriented pyrolytic graphite (HOPG), fibers, carbon foam, and carbon nanotubes (CNTs). Through the variation of gas composition and experimental parameters, the method of laser-induced pyrolysis allows the generation of carbonaceous nanostructures with different morphologies, such as, fullerene, nanoparticles with controllable structure or carbon nanotubes, providing useful functional properties. In this context, the first detection of fullerene was obtained by Ebreeht et al. in 1993, with the laser pyrolysis of acetylene-sulfur hexafluoride mixtures using in situ diagnostic with a time-of-flight mass spectrometer [188]. After that, significant amounts of fullerenes were produced, isolated and characterized by Voicu et al. in 1996 [189]. As early effort, is necessary to mention the work of Bi et al. [190] which used $CO_2$ laser pyrolysis of benzene-iron pentacarbonyl- ethylene mixture for carbon blacks production. Later works in this area were driven mainly by Cauchetier and co-workers [191]. They produced fullerenes and soot carbon by laser pyrolysis of ethylene/acetylene mixtures [192] or bencene [189] and also studied the effect of $SF_6$ addition in the laser synthesis of fullerene and soot from $C_6H_6/O_2$ or $C_6H_6/N_2O$ sensitized mixtures [193]. The C/O atomic ratio in the precursor mixture was shown to influence strongly the fullerene yield. The highest yields were obtained for a C/O ratio close to 1.2, as in combustion experiments.

Residence time in the flame is a sensitive parameter which could lead to appreciable variations of higher fullerenes yield (beyond C70) [194], as consequence, the time required for fullerene formation, it could be modulated experimentally to increase the fullerene yield and particularly higher fullerenes. [191]. Tenegal et al. synthesized fullerens by laser driven-gas phase pyrolysis from butadiene-based mixtures and demonstrated that the lowest residence times were more favourable to C60 and C70 formation as suggested in the benzene-based system. Low pressures were also found to favour the C60 and C70 formation in agreement with thermodynamic predictions. Laser pyrolysis also allowed the direct synthesis of carbon based nanoparticles with various and controllable structures: amorphous [195], turbostratic [33, 195, 196], or those which contain long packed graphene ribbons randomly [197] or concentrically oriented (forming a shell) [198]. Recently, Fleaca el al. [199] reported Fe-inserted and shell-shaped carbon nanoestructures which might be useful in applications such as MRI applications, drug

delivery or catalysts. The laser beam decomposed (via $C_2H_4$ sensitizer) the $Fe(CO)_5$ as Fe clusters which absorbed themselves the laser radiation. They triggered the fast carbon particles formation by exothermic dehydrogenation/polymerization of the surrounded $C_2H_2$ molecules. This combination between Fe clusters and $C_2H_2$ generated nanoparticles with unusual structure. Depending on the gas pressure in the reaction chamber were obtained; particles with a defective structure, a shell-shape structure, other with a turbostratic arrangement, and few containing one or several smaller (3–20 nm) Fe nanoparticles trapped inside.

Laser pyrolysis technique has also been applied to the synthesis of carbon nanotubes. Remarkable work in this field has been carried out by R Alexandrescu et al [33, 200, 201]. They reported on the synthesis of carbon nanotubes by laser-assisted technology. Hence, sensitized mixtures of iron pentacarbonyl vapour and acetylene were pyrolyzed in a flow reactor directed onto a silicon substrate. The method involved the heating of both the gas phase and the substrate by IR radiation. The carbon nanotubes were formed via the catalyzing action of the fine iron particles produced in the same experiment by the decomposition of the organometallic precursor molecules. They also used nano-iron cores embedded in carbon layers synthesized by laser pyrolysis for the growth of carbon nanofibres [201]. The flexibility of the laser pyrolysis technique has also made possible to synthesize nanocomposites, such as, core-shell nanoparticles with iron core embedded in carboxilosane polymer [202]. Alexandrescu and co-workers applied successfully these nanocomposites to vertically grow aligned CNTs on Si (100) substrates using iron–carboxysiloxane polymer nanoparticles as catalyst and a hot filament plasma-enhanced chemical vapor deposition method[203, 204].

## Conclusions

The high area/volume ratios and the significantly reduced diffusion distance in microfluidic devices are the most commonly known advantages that are attractive enough to persuade nanomaterial producers to adapt their synthesis protocols at a microfluidic scale. Continuous flow reactors based on microfluidics constitute an upcoming technology of highest potential for liquid phase synthesis of nanomaterials since it has been proposed to overcome the inherent drawbacks which batch synthesis reactor suffers from. Microreactor technology has the capacity to transform current batch nanoproduction approaches into continuous processes with rapid, uniform mixing and precise temperature control. It is expected that new advances in microfluidic reactor using the scale-up and scale-out concepts, can clearly give rise to nanoproduction under a high throughput in order to surpass conventional methods. These facts will enable to better control the properties of nanomaterials, and therefore their quality.

The laser pyrolysis method for the synthesis of nanoparticles has proven to be a flexible and versatile technique which permits finely tune nanoparticles composition, morphologies and properties for a variety of applications in challenging research fields and competitive industrial sectors. Recently, applications in the field of functional nanomaterials for optoelectronics, photonics and bio-imaging have been started. Actual plans include feasibility studies for new challenging applications, such as, the development of highly uniform doped and pure nanoparticles of complex compositions containing zero-valence metals, to develop and commercialize a range of products for applications in critical sectors like energy generation and saving. Increasing attention will be paid to initiatives aimed at applications in field with environmental/health requirements.

## Acknowledgements

Financial support from the CIBER-BBN (initiative funded by the VI National R+I Plan 2008-2011, Iniciativa Ingenio 2010, Consolider Program, CIBER Actions and financed by the Instituto de Salud Carlos III with assistance from the European Regional Development Fund) is gratefully acknowledged. The authors also thank funding from the People Program (under Marie Curie Grant agreements 321642-PLATFOMR2NANO and 294094-NANOLIGHT). JLH also thanks for a "Juan de la Cierva" Postdoctoral Fellowship from the Spanish Ministry of Science and Education.

## References

1. O. Masala and R. Seshadri, *Annual Review of Materials Research*, 2004, **34**, 41-81.
2. S. Marre and K. F. Jensen, *Chem. Soc. Rev.*, 2010, **39**, 1183-1202.
3. V. Sebastian, M. Arruebo and J. Santamaria, *Small*, 2013, n/a-n/a.
4. C. H. Chang, B. K. Paul, V. T. Remcho, S. Atre and J. E. Hutchison, *Journal of Nanoparticle Research*, 2008, **10**, 965-980.
5. E. L. C. Seris, G. Abramowitz, A. M. Johnston and B. S. Haynes, *Chemical Engineering Journal*, 2008, **135**, S9-S16.
6. V. Sebastian, S. K. Lee, C. Zhou, M. F. Kraus, J. G. Fujimoto and K. F. Jensen, *Chem. Commun.*, 2012, **48**, 6654-6656.
7. S. Krishnadasan, R. J. C. Brown, A. J. deMello and J. C. deMello, *Lab on a Chip*, 2007, **7**, 1434-1441.
8. O. Levenspiel, *Chemical Engineering Science*, 2002, **57**, 4691-4696.
9. H. Nakamura, Y. Yamaguchi, M. Miyazaki, H. Maeda, M. Uehara and P. Mulvaney, *Chem. Commun.*, 2002, 2844-2845.
10. V. S. Cabeza, S. Kuhn, A. A. Kulkarni and K. F. Jensen, *Langmuir*, 2012, **28**, 7007-7013.
11. K. S. Krishna, Y. Li, S. Li and C. S. S. R. Kumar, *Advanced Drug Delivery Reviews*, 2013, **65**, 1470-1495.
12. J. X. Ju, C. F. Zeng, L. X. Zhang and N. P. Xu, *Chemical Engineering Journal*, 2006, **116**, 115-121.
13. P. S. Dittrich, K. Tachikawa and A. Manz, *Anal. Chem.*, 2006, **78**, 3887-3907.
14. T. McCreedy, *Trac-Trends in Analytical Chemistry*, 2000, **19**, 396-401.
15. K. F. Jensen, *Chemical Engineering Science*, 2001, **56**, 293-303.
16. D. M. Ratner, E. R. Murphy, M. Jhunjhunwala, D. A. Snyder, K. F. Jensen and P. H. Seeberger, *Chem. Commun.*, 2005, 578-580.
17. V. Hessel, H. Lowe and F. Schonfeld, *Chemical Engineering Science*, 2005, **60**, 2479-2501.
18. V. Sebastian, O. de la Iglesia, R. Mallada, L. Casado, G. Kolb, V. Hessel and J. Santamaria, *Microporous Mesoporous Mat.*, 2008, **115**, 147-155.
19. V. Hessel, S. Hardt, H. Lowe and F. Schonfeld, *Aiche J.*, 2003, **49**, 566-577.
20. P. Lob, K. S. Drese, V. Hessel, S. Hardt, C. Hofmann, H. Lowe, R. Schenk, F. Schonfeld and B. Werner, *Chem. Eng. Technol.*, 2004, **27**, 340-345.
21. S. Y. Yang, F. Y. Cheng, C. S. Yeh and G. B. Lee, *Microfluidics and Nanofluidics*, 2010, **8**, 303-311.
22. J. C. McDonald, D. C. Duffy, J. R. Anderson, D. T. Chiu, H. K. Wu, O. J. A. Schueller and G. M. Whitesides, *Electrophoresis*, 2000, **21**, 27-40.
23. Y. J. Song, C. S. S. R. Kumar and J. Hormes, *J. Micromech. Microeng.*, 2004, **14**, 932-940.

24. R. Zengerle, J. Ulrich, S. Kluge, M. Richter and A. Richter, *Sensors and Actuators a-Physical*, 1995, **50**, 81-86.
25. M. Capanu, J. G. Boyd and P. J. Hesketh, *Journal of Microelectromechanical Systems*, 2000, **9**, 181-189.
26. K. L. Zhang, S. K. Chou and S. S. Ang, *International Journal of Thermal Sciences*, 2007, **46**, 580-588.
27. S. Krishnadasan, A. Yashina, A. J. deMello and J. C. deMello, *Microsystems and Devices for (Bio)Chemical Processes*, 2010, **38**, 195-231.
28. N. Schwesinger, T. Frank and H. Wurmus, *J. Micromech. Microeng.*, 1996, **6**, 99-102.
29. W. R. Cannon, S. C. Danforth, J. H. Flint, J. S. Haggerty and R. A. Marra, *Journal of the American Ceramic Society*, 1982, **65**, 324-330.
30. M. A. Duncan, T. G. Dietz and R. E. Smalley, *J. Am. Chem. Soc.*, 1981, **103**, 5245-5246.
31. K. E. Lewis, D. M. Golden and G. P. Smith, *J. Am. Chem. Soc.*, 1984, **106**, 3905-3912.
32. M. T. Swihart, *Current Opinion in Colloid & Interface Science*, 2003, **8**, 127-133.
33. I. Morjan, I. Voicu, F. Dumitrache, I. Sandu, I. Soare, R. Alexandrescu, E. Vasile, I. Pasuk, R. M. D. Brydson, H. Daniels and B. Rand, *Carbon*, 2003, **41**, 2913-2921.
34. X. Li, Y. He, S. S. Talukdar and M. T. Swihart, *Langmuir*, 2003, **19**, 8490-8496.
35. T. Majima, Y. Matsumoto and M. Takami, *Journal of Photochemistry and Photobiology A: Chemistry*, 1993, **71**, 213-219.
36. S. Chiruvolu, *Internal Report NanoGram Corparation*, 1999.
37. B. Elisabetta, B. Sabina, C. Luisa, D. Luigi De and F. Roberta, *Physica Scripta*, 2008, **78**, 058112.
38. G. Martínez, A. Malumbres, R. Mallada, J. L. Hueso, S. Irusta, O. Bomatí-Miguel and J. Santamaría, *Nanotechnology*, 2012, **23**, 425605.
39. A. Malumbres, G. Martínez, R. Mallada, J. L. Hueso, O. Bomatí-Miguel and J. Santamaría, *Nanotechnology*, 2013, **24**, 325603.
40. C. X. Zhao, L. Z. He, S. Z. Qiao and A. P. J. Middelberg, *Chemical Engineering Science*, 2011, **66**, 1463-1479.
41. J. DeMello and A. DeMello, *Lab on a Chip*, 2004, **4**, 11n-15n.
42. A. Gunther, S. A. Khan, M. Thalmann, F. Trachsel and K. F. Jensen, *Lab on a Chip*, 2004, **4**, 278-286.
43. S. A. Khan and K. F. Jensen, *Advanced Materials*, 2007, **19**, 2556-+.
44. R. L. Hartman, H. R. Sahoo, B. C. Yen and K. F. Jensen, *Lab on a Chip*, 2009, **9**, 1843-1849.
45. J. Baek, P. M. Allen, M. G. Bawendi and K. F. Jensen, *Angew. Chem.-Int. Edit.*, 2011, **50**, 627-630.
46. J. B. Edel, R. Fortt, J. C. deMello and A. J. deMello, *Chem. Commun.*, 2002, 1136-1137.
47. C. Y. Lee, C. L. Chang, Y. N. Wang and L. M. Fu, *International Journal of Molecular Sciences*, 2011, **12**, 3263-3287.
48. Z. Yang, S. Matsumoto, H. Goto, M. Matsumoto and R. Maeda, *Sensors and Actuators a-Physical*, 2001, **93**, 266-272.
49. M. Campisi, D. Accoto, F. Damiani and P. Dario, *Journal of Micro-Nano Mechatronics*, 2009, **5**, 69-76.
50. X. Z. Niu and Y. K. Lee, *J. Micromech. Microeng.*, 2003, **13**, 454-462.
51. A. O. El Moctar, N. Aubry and J. Batton, *Lab on a Chip*, 2003, **3**, 273-280.
52. H. H. Bau, J. H. Zhong and M. Q. Yi, *Sensors and Actuators B-Chemical*, 2001, **79**, 207-215.
53. B. He, B. J. Burke, X. Zhang, R. Zhang and F. E. Regnier, *Anal. Chem.*, 2001, **73**, 1942-1947.
54. J. Melin, G. Gimenez, N. Roxhed, W. van der Wijngaart and G. Stemme, *Lab on a Chip*, 2004, **4**, 214-219.

55. V. Mengeaud, J. Josserand and H. H. Girault, *Anal. Chem.*, 2002, **74**, 4279-4286.
56. Y. J. Song, J. Hormes and C. S. S. R. Kumar, *Small*, 2008, **4**, 698-711.
57. J. Wagner and J. M. Kohler, *Nano Lett.*, 2005, **5**, 685-691.
58. L. Gomez, V. Sebastian, S. Irusta, A. Ibarra, M. Arruebo and J. Santamaria, *Lab on a Chip*, 2014, **14**, 325-332.
59. K. J. Hartlieb, M. Saunders, R. J. J. Jachuck and C. L. Raston, *Green Chemistry*, 2010, **12**, 1012-1017.
60. J. Boleininger, A. Kurz, V. Reuss and C. Sonnichsen, *Physical Chemistry Chemical Physics*, 2006, **8**, 3824-3827.
61. S. Duraiswamy and S. A. Khan, *Small*, 2009, **5**, 2828-2834.
62. A. Knauer, A. Csaki, F. Moller, C. Huhn, W. Fritzsche and J. M. Kohler, *J. Phys. Chem. C*, 2012, **116**, 9251-9258.
63. Y. J. Song, E. E. Doomes, J. Prindle, R. Tittsworth, J. Hormes and C. S. S. R. Kumar, *Journal of Physical Chemistry B*, 2005, **109**, 9330-9338.
64. L. Frenz, A. El Harrak, M. Pauly, S. Begin-Colin, A. D. Griffiths and J. C. Baret, *Angew. Chem.-Int. Edit.*, 2008, **47**, 6817-6820.
65. S. A. Khan, A. Gunther, M. A. Schmidt and K. F. Jensen, *Langmuir*, 2004, **20**, 8604-8611.
66. L. Gutierrez, L. Gomez, S. Irusta, M. Arruebo and J. Santamaria, *Chemical Engineering Journal*, 2011, **171**, 674-683.
67. B. F. Cottam, S. Krishnadasan, A. J. deMello, J. C. deMello and M. S. P. Shaffer, *Lab on a Chip*, 2007, **7**, 167-169.
68. S. Li, S. Meierott and J. M. Kohler, *Chemical Engineering Journal*, 2010, **165**, 958-965.
69. H. W. Yang, W. L. Luan, S. T. Tu and Z. M. M. Wang, *Lab on a Chip*, 2008, **8**, 451-455.
70. B. K. H. Yen, A. Gunther, M. A. Schmidt, K. F. Jensen and M. G. Bawendi, *Angew. Chem.-Int. Edit.*, 2005, **44**, 5447-5451.
71. B. K. H. Yen, N. E. Stott, K. F. Jensen and M. G. Bawendi, *Advanced Materials*, 2003, **15**, 1858-1862.
72. S. Krishnadasan, J. Tovilla, R. Vilar, A. J. deMello and J. C. deMello, *Journal of Materials Chemistry*, 2004, **14**, 2655-2660.
73. E. M. Chan, A. P. Alivisatos and R. A. Mathies, *J. Am. Chem. Soc.*, 2005, **127**, 13854-13861.
74. L. H. Hung, K. M. Choi, W. Y. Tseng, Y. C. Tan, K. J. Shea and A. P. Lee, *Lab on a Chip*, 2006, **6**, 174-178.
75. S. Marre, J. Park, J. Rempel, J. Guan, M. G. Bawendi and K. F. Jensen, *Advanced Materials*, 2008, **20**, 4830-+.
76. H. Z. Wang, X. Y. Li, M. Uehara, Y. Yamaguchi, H. Nakamura, M. P. Miyazaki, H. Shimizu and H. Maeda, *Chem. Commun.*, 2004, 48-49.
77. A. Knauer, A. Thete, S. Li, H. Romanus, A. Csaki, W. Fritzsche and J. M. Kohler, *Chemical Engineering Journal*, 2011, **166**, 1164-1169.
78. S. K. Lee, X. Y. Liu, V. S. Cabeza and K. F. Jensen, *Lab on a Chip*, 2012, **12**, 4080-4084.
79. Y. J. Zhao, H. C. Shum, H. S. Chen, L. L. A. Adams, Z. Z. Gu and D. A. Weitz, *J. Am. Chem. Soc.*, 2011, **133**, 8790-8793.
80. J. Y. Chang, C. H. Yang and K. S. Huang, *Nanotechnology*, 2007, **18**.
81. J. Gascon, F. Kapteijn, B. Zornoza, V. Sebastian, C. Casado and J. Coronas, *Chemistry of Materials*, 2012, **24**, 2829-2844.
82. P. H. Hoang, H. Park and D. P. Kim, *J. Am. Chem. Soc.*, 2011, **133**, 14765-14770.
83. Y. C. Pan, J. F. Yao, L. X. Zhang and N. P. Xu, *Industrial & Engineering Chemistry Research*, 2009, **48**, 8471-8477.

84. Y. C. Pan, M. H. Ju, J. F. Yao, L. X. Zhang and N. P. Xu, *Chem. Commun.*, 2009, 7233-7235.
85. F. Castro, S. Kuhn, K. Jensen, A. Ferreira, F. Rocha, A. Vicente and J. A. Teixeira, *Chemical Engineering Journal*, 2013, **215–216**, 979-987.
86. R. A. Petros and J. M. DeSimone, *Nature Reviews Drug Discovery*, 2010, **9**, 615-627.
87. A. Jahn, J. E. Reiner, W. N. Vreeland, D. L. DeVoe, L. E. Locascio and M. Gaitan, *Journal of Nanoparticle Research*, 2008, **10**, 925-934.
88. K. Kuribayashi, G. Tresset, P. Coquet, H. Fujita and S. Takeuchi, *Measurement Science & Technology*, 2006, **17**, 3121-3126.
89. A. Wagner, K. Vorauer-Uhl, G. Kreismayr and H. Katinger, *Journal of Liposome Research*, 2002, **12**, 259-270.
90. A. Jahn, W. N. Vreeland, M. Gaitan and L. E. Locascio, *J. Am. Chem. Soc.*, 2004, **126**, 2674-2675.
91. C. X. Zhao, *Advanced Drug Delivery Reviews*, 2013, **65**, 1420-1446.
92. V. Barbier, M. Tatoulian, H. Li, F. Arefi-Khonsari, A. Ajdari and P. Tabeling, *Langmuir*, 2006, **22**, 5230-5232.
93. S. Okushima, T. Nisisako, T. Torii and T. Higuchi, *Langmuir*, 2004, **20**, 9905-9908.
94. R. K. Shah, J. W. Kim, J. J. Agresti, D. A. Weitz and L. Y. Chu, *Soft Matter*, 2008, **4**, 2303-2309.
95. M. Bouquey, C. Serra, N. Berton, L. Prat and G. Hadziioannou, *Chemical Engineering Journal*, 2008, **135**, S93-S98.
96. P. Panizza, W. Engl, C. Hany and R. Backov, *Colloids and Surfaces a-Physicochemical and Engineering Aspects*, 2008, **312**, 24-31.
97. K. W. Bong, D. C. Pregibon and P. S. Doyle, *Lab on a Chip*, 2009, **9**, 863-866.
98. R. Karnik, F. Gu, P. Basto, C. Cannizzaro, L. Dean, W. Kyei-Manu, R. Langer and O. C. Farokhzad, *Nano Lett.*, 2008, **8**, 2906-2912.
99. D. J. L. a. F. D., *Magnetic Propertiesof Fine Particles*, North-Holland, 1992.
100. C. Kittel, *Physical Review*, 1946, **70**, 965-971.
101. E. M. Chudnovsky and L. Gunther, *Physical Review B*, 1988, **37**, 9455-9459.
102. E. M. Chudnovsky and L. Gunther, *Physical Review Letters*, 1988, **60**, 661-664.
103. R. M. a. S. U. Cornell, *The iron oxides*, VCH, Weinheim, 1996.
104. W. Weiss and W. Ranke, *Progress in Surface Science*, 2002, **70**, 1-151.
105. M. J. Hampden-Smith and T. T. Kodas, *Chem. Vapor Depos.*, 1995, **1**, 8-23.
106. R. Alexandrescu, *Appl. Surf. Sci.*, 1996, **106**, 28-37.
107. G. P. Smith and R. M. Laine, *The Journal of Physical Chemistry*, 1981, **85**, 1620-1622.
108. I. Morjan, R. Alexandrescu, I. Soare, F. Dumitrache, I. Sandu, I. Voicu, A. Crunteanu, E. Vasile, V. Ciupina and S. Martelli, *Materials Science and Engineering: C*, 2003, **23**, 211-216.
109. C. S. C. R. Alexandrescu, A. Crunteanu, I. Morjan, I. Voicu, F. Huiken, B. Kohn, F. Vasiliu, D. Fatu, *Synthesis of iron carbide-based nanopowders by laser photoinduced reactions from gaseous precursors*, 1999.
110. Y. He, Y. Sahoo, S. Wang, H. Luo, P. Prasad and M. Swihart, *Journal of Nanoparticle Research*, 2006, **8**, 335-342.
111. S. Veintemillas-Verdaguer, M. P. Morales and C. J. Serna, *Materials Letters*, 1998, **35**, 227-231.
112. S. V.-V. a. C. J. S. M. P. Morales, *Journal of Materials Research*, 1999, **14**.
113. M. P. Morales, S. Veintemillas-Verdaguer, M. I. Montero, C. J. Serna, A. Roig, L. Casas, B. Martínez and F. Sandiumenge, *Chemistry of Materials*, 1999, **11**, 3058-3064.
114. S. Martelli, A. Mancini, R. Giorgi, R. Alexandrescu, S. Cojocaru, A. Crunteanu, I. Voicu, M. Balu and I. Morjan, *Appl. Surf. Sci.*, 2000, **154–155**, 353-359.

115.S. Veintemillas-Verdaguer, O. Bomatí-Miguel and M. P. Morales, *Scripta Materialia*, 2002, **47**, 589-593.
116.M. P. Morales, M. Andres-Vergés, S. Veintemillas-Verdaguer, M. I. Montero and C. J. Serna, *Journal of Magnetism and Magnetic Materials*, 1999, **203**, 146-148.
117.C. J. Serna, F. Bødker, S. Mørup, M. P. Morales, F. Sandiumenge and S. Veintemillas-Verdaguer, *Solid State Communications*, 2001, **118**, 437-440.
118.R. Costo, V. Bello, C. Robic, M. Port, J. F. Marco, M. Puerto Morales and S. Veintemillas-Verdaguer, *Langmuir*, 2011, **28**, 178-185.
119.M. C. Bautista, O. Bomati-Miguel, X. Zhao, M. P. Morales, T. González-Carreño, R. P. d. Alejo, J. Ruiz-Cabello and S. Veintemillas-Verdaguer, *Nanotechnology*, 2004, **15**, S154.
120.V.-V. Sabino, M. Maria del Puerto, B.-M. Oscar, B. Carmen, Z. Xinqing, B. Pierre, A. Rigoberto Pérez de, R.-C. Jesus, S. Martin, J. T.-C. Francisco and F. Joaquin, *Journal of Physics D: Applied Physics*, 2004, **37**, 2054.
121.O. Bomatí-Miguel, M. P. Morales, P. Tartaj, J. Ruiz-Cabello, P. Bonville, M. Santos, X. Zhao and S. Veintemillas-Verdaguer, *Biomaterials*, 2005, **26**, 5695-5703.
122.A. Marcu, S. Pop, F. Dumitrache, M. Mocanu, C. M. Niculite, M. Gherghiceanu, C. P. Lungu, C. Fleaca, R. Ianchis, A. Barbut, C. Grigoriu and I. Morjan, *Appl. Surf. Sci.*, 2013, **281**, 60-65.
123.E. Popovici, F. Dumitrache, I. Morjan, R. Alexandrescu, V. Ciupina, G. Prodan, L. Vekas, D. Bica, O. Marinica and E. Vasile, *Appl. Surf. Sci.*, 2007, **254**, 1048-1052.
124.J. F. Bosh H., *Catalysis Today*, 1988, **2**, 369-379.
125.P. Forzatti, *Catalysis Today*, 2000, **62**, 51-65.
126.M. R. Hoffmann, S. T. Martin, W. Choi and D. W. Bahnemann, *Chemical Reviews*, 1995, **95**, 69-96.
127.A. Maldotti, A. Molinari and R. Amadelli, *Chemical Reviews*, 2002, **102**, 3811-3836.
128.K. G. Kalyanasendevan, *Optoelectrinics Properties of Inorganic Compounds*, Plenum, New York, 1999.
129.P. Bonhôte, E. Gogniat, M. Grätzel and P. V. Ashrit, *Thin Solid Films*, 1999, **350**, 269-275.
130.L. G. Phillips and D. M. Barbano, *Journal of dairy science*, 1997, **80**, 2726-2731.
131.S. H, *Vacuum Thin Films*, 1999, 15.
132.A. Fujishima, T. N. Rao and D. A. Tryk, *Journal of Photochemistry and Photobiology C: Photochemistry Reviews*, 2000, **1**, 1-21.
133.H.-J. Zhai and L.-S. Wang, *J. Am. Chem. Soc.*, 2007, **129**, 3022-3026.
134.Z.-w. Qu and G.-J. Kroes, *The Journal of Physical Chemistry B*, 2006, **110**, 8998-9007.
135.X. Bokhimi, A. Morales, O. Novaro, T. López, O. Chimal, M. Asomoza and R. Gómez, *Chemistry of Materials*, 1997, **9**, 2616-2620.
136.H. Zhang and J. F. Banfield, *Journal of Materials Chemistry*, 1998, **8**, 2073-2076.
137.J. D. Casey and J. Haggerty, *Journal of Materials Science*, 1987, **22**, 4307-4312.
138.F. Curcio, M. Musci, N. Notaro and G. De Michele, *Appl. Surf. Sci.*, 1990, **46**, 225-229.
139.M. Musci, M. Notaro, F. Curcio, C. Casale and G. De Michele, *J. Mater. Res.*, 1992, **7**, 2846-2852.
140.L. E. Depero, P. Bonzi, M. Musci and C. Casale, *Journal of Solid State Chemistry*, 1994, **111**, 247-252.
141.L. S. L.E. Depero, B. Allieri, F. Pioselli, C. Casale, and M. Notaro, *Mater. Sci. Forum*, 1998, **278–281**, 654.
142.L. E. Depero, L. Sangaletti, B. Allieri, E. Bontempi, R. Salari, M. Zocchi, C. Casale and M. Notaro, *J. Mater. Res.*, 1998, **13**, 1644-1649.

143.L. E. Depero, A. Marino, B. Allieri, E. Bontempi, L. Sangaletti, C. Casale and M. Notaro, *J. Mater. Res.*, 2000, **15**, 2080-2086.
144.R. Alexandrescu, I. Morjan, M. Scarisoreanu, R. Birjega, E. Popovici, I. Soare, L. Gavrila-Florescu, I. Voicu, I. Sandu, F. Dumitrache, G. Prodan, E. Vasile and E. Figgemeier, *Thin Solid Films*, 2007, **515**, 8438-8445.
145.J. Arbiol, J. Cerdà, G. Dezanneau, A. Cirera, F. Peiró, A. Cornet and J. R. Morante, *J. Appl. Phys.*, 2002, **92**, 853-861.
146.R. Alexandrescu, F. Dumitrache, I. Morjan, I. Sandu, M. Savoiu, I. Voicu, C. Fleaca and R. Piticescu, *Nanotechnology*, 2004, **15**, 537.
147.B. Pignon, H. Maskrot, V. Guyot Ferreol, Y. Leconte, S. Coste, M. Gervais, T. Pouget, C. Reynaud, J.-F. Tranchant and N. Herlin-Boime, *European Journal of Inorganic Chemistry*, 2008, **2008**, 883-889.
148.M. Scarisoreanu, Morjan, R. Alexandrescu, R. Birjega, I. Voicu, C. Fleaca, E. Popovici, I. Soare, L. Gavrila-Florescu, O. Cretu, G. Prodan, V. Ciupina and E. Figgemeier, *Appl. Surf. Sci.*, 2007, **253**, 7908-7911.
149.E. Figgemeier, W. Kylberg, E. Constable, M. Scarisoreanu, R. Alexandrescu, I. Morjan, I. Soare, R. Birjega, E. Popovici, C. Fleaca, L. Gavrila-Florescu and G. Prodan, *Appl. Surf. Sci.*, 2007, **254**, 1037-1041.
150.T. Kauffeldt, H. Lakner, M. Lohmann and A. Schmidt-Ott, *Nanostructured Materials*, 1995, **6**, 365-368.
151.M. Scarisoreanu, R. Alexandrescu, I. Morjan, R. Birjega, C. Luculescu, E. Popovici, E. Dutu, E. Vasile, V. Danciu and N. Herlin-Boime, *Appl. Surf. Sci.*, 2013, **278**, 295-300.
152.R. Alexandrescu, M. Scarisoreanu, I. Morjan, R. Birjega, C. Fleaca, C. Luculescu, I. Soare, O. Cretu, C. C. Negrila, N. Lazarescu and V. Ciupina, *Appl. Surf. Sci.*, 2009, **255**, 5373-5377.
153.P. Simon, B. Pignon, B. Miao, S. Coste-Leconte, Y. Leconte, S. Marguet, P. Jegou, B. Bouchet-Fabre, C. Reynaud and N. Herlin-Boime, *Chemistry of Materials*, 2010, **22**, 3704-3711.
154.R. Asahi, T. Morikawa, T. Ohwaki, K. Aoki and Y. Taga, *Science*, 2001, **293**, 269-271.
155.C. Burda, Y. Lou, X. Chen, A. C. S. Samia, J. Stout and J. L. Gole, *Nano Lett.*, 2003, **3**, 1049-1051.
156.M. Sathish, B. Viswanathan, R. P. Viswanath and C. S. Gopinath, *Chemistry of Materials*, 2005, **17**, 6349-6353.
157.H. Melhem, P. Simon, J. Wang, C. Di Bin, B. Ratier, Y. Leconte, N. Herlin-Boime, M. Makowska-Janusik, A. Kassiba and J. Bouclé, *Sol. Energy Mater. Sol. Cells*, 2013, **117**, 624-631.
158.J. A. Rodrígez, Fernández-Garcia, M, *Synthesis, Properties and Applications of Oxide Nanoparticles*, Whiley, New Jersey, 2007.
159.G. C. a. M.-A. Mather, A., *Transport properties and Oxigen Handling* Whiley, New Jersey, 2007.
160.A. A. J. M. McHale, A. J. Perrotta, A. Navrotsky, *Science* 1997, **277**.
161.E. Borsella, S. Botti, R. Giorgi, S. Martelli, S. Turtù and G. Zappa, *Appl. Phys. Lett.*, 1993, **63**, 1345-1347.
162.R. Alexandrescu, E. Borsella, S. Botti, M. P. Cesile, S. Martelli, R. Giorgi, S. Turtù and G. Zappa, *J. Mater. Res.*, 1997, **12**, 774-782.
163.C. Bittencourt, R. Landers, E. Llobet, G. Molas, X. Correig, M. A. P. Silva, J. E. Sueiras and J. Calderer, *Journal of The Electrochemical Society*, 2002, **149**, H81-H86.
164.H. Kawasaki, J. Namba, K. Iwatsuji, Y. Suda, K. Wada, K. Ebihara and T. Ohshima, *Appl. Surf. Sci.*, 2002, **197–198**, 547-551.
165.S.-H. Wang, T.-C. Chou and C.-C. Liu, *Sensors and Actuators B: Chemical*, 2003, **94**, 343-351.

166.B. W. Mwakikunga, A. Forbes, E. Sideras-Haddad, R. M. Erasmus, G. Katumba and B. Masina, *International Journal of Nanoparticles*, 2008, **1**, 185-202.
167.B. Mwakikunga, A. Forbes, E. Sideras-Haddad and C. Arendse, *Nanoscale Research Letters*, 2008, **3**, 372 - 380.
168.M. Govender, L. Shikwambana, B. Mwakikunga, E. Sideras-Haddad, R. Erasmus and A. Forbes, *Nanoscale Research Letters*, 2011, **6**, 166.
169.J. A. Kern, H. G. Schwahn and B. Schramm, *Materials Chemistry and Physics*, 1989, **21**, 391-408.
170.G. Peters, K. Jerg and B. Schramm, *Materials Chemistry and Physics*, 1998, **55**, 197-201.
171.Y. He, X. Li and M. T. Swihart, *Chemistry of Materials*, 2005, **17**, 1017-1026.
172.J. P. Wilcoxon, G. A. Samara and P. N. Provencio, *Physical Review B*, 1999, **60**, 2704-2714.
173.F. Erogbogbo, K.-T. Yong, R. Hu, W.-C. Law, H. Ding, C.-W. Chang, P. N. Prasad and M. T. Swihart, *ACS Nano*, 2010, **4**, 5131-5138.
174.F. Erogbogbo, K.-T. Yong, I. Roy, R. Hu, W.-C. Law, W. Zhao, H. Ding, F. Wu, R. Kumar, M. T. Swihart and P. N. Prasad, *ACS Nano*, 2010, **5**, 413-423.
175.A. Gupta, M. T. Swihart and H. Wiggers, *Advanced Functional Materials*, 2009, **19**, 696-703.
176.C. M. Hessel, M. R. Rasch, J. L. Hueso, B. W. Goodfellow, V. A. Akhavan, P. Puvanakrishnan, J. W. Tunnel and B. A. Korgel, *Small*, 2010, **6**, 2026-2034.
177.E. Borsella, M. Falconieri, S. Botti, S. Martelli, F. Bignoli, L. Costa, S. Grandi, L. Sangaletti, B. Allieri and L. Depero, *Materials Science and Engineering: B*, 2001, **79**, 55-62.
178.S. Botti, R. Coppola, F. Gourbilleau and R. Rizk, *J. Appl. Phys.*, 2000, **88**, 3396-3401.
179.F. Huisken, B. Kohn and V. Paillard, *Appl. Phys. Lett.*, 1999, **74**, 3776-3778.
180.M. Ehbrecht, B. Kohn, F. Huisken, M. A. Laguna and V. Paillard, *Physical Review B*, 1997, **56**, 6958-6964.
181.G. Ledoux, J. Gong, F. Huisken, O. Guillois and C. Reynaud, *Appl. Phys. Lett.*, 2002, **80**, 4834-4836.
182.G. Ledoux, J. Gong and F. Huisken, *Appl. Phys. Lett.*, 2001, **79**, 4028-4030.
183.M. Modreanu, M. Gartner and D. Cristea, *Materials Science and Engineering: C*, 2002, **19**, 225-228.
184.X. Li, Y. He and M. T. Swihart, *Langmuir*, 2004, **20**, 4720-4727.
185.P. E. Di Nunzio and S. Martelli, *Aerosol Science and Technology*, 2006, **40**, 724-734.
186.F. Lacour, O. Guillois, X. Portier, H. Perez, N. Herlin and C. Reynaud, *Physica E: Low-dimensional Systems and Nanostructures*, 2007, **38**, 11-15.
187.O. Sublemontier, F. Lacour, Y. Leconte, N. Herlin-Boime and C. Reynaud, *Journal of Alloys and Compounds*, 2009, **483**, 499-502.
188.M. Ehbrecht, M. Faerber, F. Rohmund, V. V. Smirnov, O. Stelmakh and F. Huisken, *Chemical Physics Letters*, 1993, **214**, 34-38.
189.I. Voicu, X. Armand, M. Cauchetier, N. Herlin and S. Bourcier, *Chemical Physics Letters*, 1996, **256**, 261-268.
190.X.-X. Bi, M. Jagtoyen, M. Endo, K. Das Chowdhury, R. Ochoa, F. J. Derbyshire, M. S. Dresselhaus and P. C. Eklund, *J. Mater. Res.*, 1995, **10**, 2875-2884.
191.F. Ténégal, I. Voicu, X. Armand, N. Herlin-Boime and C. Reynaud, *Chemical Physics Letters*, 2003, **379**, 40-46.
192.X. Armand, N. Herlin, I. Voicu and M. Cauchetier, *Journal of Physics and Chemistry of Solids*, 1997, **58**, 1853-1859.
193.R. Alexandrescu, X. Armand, M. Cauchetier, N. Herlin, S. Petcu and I. Voicu, *Carbon*, 1998, **36**, 1285-1290.

194.C. J. Pope, J. A. Marr and J. B. Howard, *The Journal of Physical Chemistry*, 1993, **97**, 11001-11013.
195.A. Galvez, N. Herlin-Boime, C. Reynaud, C. Clinard and J.-N. Rouzaud, *Carbon*, 2002, **40**, 2775-2789.
196.I. Morjan, I. Voicu, R. Alexandrescu, I. Pasuk, I. Sandu, F. Dumitrache, I. Soare, T. C. Fleaca, M. Ploscaru, V. Ciupina, H. Daniels, A. Westwood and B. Rand, *Carbon*, 2004, **42**, 1269-1273.
197.L. Gavrila Florescu, E. Vasile, I. Sandu, I. Soare, C. Fleaca, R. Ianchis, C. Luculescu, E. Dutu, R. Birjega, I. Morjan and I. Voicu, *Appl. Surf. Sci.*, 2011, **257**, 5270-5273.
198.M. Choi, I. S. Altman, Y. J. Kim, P. V. Pikhitsa, S. Lee, G. S. Park, T. Jeong and J. B. Yoo, *Advanced Materials*, 2004, **16**, 1721-1725.
199.C. T. Fleaca, F. Dumitrache, I. Morjan, R. Alexandrescu, I. Sandu, C. Luculescu, S. Birjega, G. Prodan and I. Stamatin, *Appl. Surf. Sci.*, 2012, **258**, 9394-9398.
200.R. Alexandrescu, A. Crunteanu, R. E. Morjan, I. Morjan, F. Rohmund, L. K. L. Falk, G. Ledoux and F. Huisken, *Infrared Physics & Technology*, 2003, **44**, 43-50.
201.F. Dumitrache, I. Morjan, R. Alexandrescu, R. E. Morjan, I. Voicu, I. Sandu, I. Soare, M. Ploscaru, C. Fleaca, V. Ciupina, G. Prodan, B. Rand, R. Brydson and A. Woodword, *Diamond and Related Materials*, 2004, **13**, 362-370.
202.J. Pola, M. Maryško, V. Vorlíček, Z. Bastl, A. Galíková, K. Vacek, R. Alexandrescu, F. Dumitrache, I. Morjan, L. Albu and G. Prodan, *Applied Organometallic Chemistry*, 2005, **19**, 1015-1021.
203.C. T. Fleaca, I. Morjan, R. Alexandrescu, F. Dumitrache, I. Soare, L. Gavrila-Florescu, F. Le Normand and O. Ersen, *Physica E: Low-dimensional Systems and Nanostructures*, 2008, **40**, 2252-2256.
204.C. T. Fleaca, I. Morjan, R. Alexandrescu, F. Dumitrache, I. Soare, L. Gavrila-Florescu, F. Le Normand and A. Derory, *Appl. Surf. Sci.*, 2009, **255**, 5386-5390.